
Q3R: Quadratic Reweighted Rank Regularizer for Effective Low-Rank Training

Ipsita Ghosh*

Department of Computer Science
University of Central Florida
ipsita.ghosh@ucf.edu

Ethan Nguyen*

Department of Computer Science
University of North Carolina at Charlotte
ethan.nguyen@e-10.net

Christian Kümmerle

School of Data, Mathematical and Statistical Sciences
Department of Computer Science
University of Central Florida
kummerle@ucf.edu

Abstract

Parameter-efficient training based on low-rank optimization has become a highly successful tool for fine-tuning large deep learning models. However, these methods often fail for low-rank pre-training, where simultaneously maintaining low-rank weight structure and optimizing the task objective remains challenging. We propose the *Quadratic Reweighted Rank Regularizer* (Q3R), which leads to a novel low-rank-inducing training strategy inspired by the iteratively reweighted least squares (IRLS) framework. Q3R is based on a quadratic regularizer term that majorizes a smoothed log-determinant rank surrogate. Unlike other low-rank training techniques, Q3R can train weight matrices to prescribed low target ranks while achieving predictive performance comparable to dense models, with small computational overhead and full compatibility with existing architectures. For example, we demonstrate a Q3R-regularized ViT-Tiny experiment where truncating the model to 60% and 80% of its parameters results in only minor absolute accuracy drops of 1.3% and 4%, respectively, on CIFAR-10. We confirm the efficacy of Q3R on Transformers across both vision and language tasks, including low-rank fine-tuning.

The code is available at <https://github.com/ThatE10/q3r.git>.

1 Introduction

Modern deep learning architectures continue to grow in size and complexity [RWC⁺19], creating a growing demand for efficient training methodologies. Low-rank regularization has emerged as a powerful paradigm for addressing these challenges by explicitly constraining the parameter search space through matrix factorization. This approach builds on the empirical observation that neural networks exhibit inherent low-dimensional structure in their weight matrices during training [GK⁺22].

Practical implementations face three key challenges: (1) performance degradation compared to full-rank baselines, (2) optimal rank selection across layers, and (3) maintaining training stability. Prior work addresses these through spectral initialization [GK⁺22], orthogonality regularization [YYT⁺20].

*Equal contribution.

Recent advances in parameter-efficient fine-tuning (PEFT) have expanded the low-rank training paradigm through methods like Low-Rank Induced Training (LoRITa) [AZW24]. These approaches maintain the original model architecture during inference while inducing low-rank structure through strategic layer overparameterization during training. LoRITa specifically decomposes weight matrices \mathbf{W}_i into products $\prod_{k=1}^N \mathbf{W}_i^k$ during optimization, enabling implicit rank reduction through singular value truncation post-training [AZW24]. This methodology demonstrates that explicit rank constraints can be replaced by training dynamics that naturally favor low-rank solutions.

Despite their promise, existing low-rank training approaches present several notable limitations. Traditional low-rank methods often suffer from performance degradation relative to full-rank baselines [GK⁺22, YYT⁺20]. Methods such as LoRA and LoRITa, while effective at reducing trainable parameters, can struggle to capture the full structure making it difficult to generalize to complex tasks [AZW24]. Furthermore, PEFT techniques introduce additional hyperparameters (such as rank and scaling factors) whose optimal values may not generalize across architectures, datasets, or downstream tasks, often requiring extensive re-tuning and experimentation. In multilingual or low-resource settings, PEFT methods like LoRA have been observed to yield inconsistent results, sometimes improving language-specific generation at the expense of reasoning or generalization abilities [KJ⁺25]. Combining multiple PEFT modules for multi-task or continual learning can also lead to increased memory usage and system complexity, offsetting some of the intended efficiency gains. Overall, it can be observed that the advances in LoRA-type parameter-efficient training methods have not yet been able to be translated to enable robust low-rank pre-training.

2 Contribution

In this paper, we propose the **Quadratic Reweighted Rank Regularizer (Q3R)**, which bridges this gap by introducing an optimizer-compatible regularization framework based on smoothed log-determinant rank surrogates outlined in Section 4.1 and specifically designed for low-rank pre-training. While theoretically grounded in saddle-escaping second-order optimization methods, it comes with little computational overhead compared to unregularized training despite its efficacy for promoting low-rank neural network weight matrices. Additionally, we propose the Adam variant AdamQ3R in Section 4.2, which is tailored to optimizing Q3R-regularized loss functions and which improves the performance of training Q3R-regularized models.

We demonstrate in numerical experiments that Q3R is able to reduce the number of parameters in ViT models by, for example, 60% during pre-training on CIFAR-10, with only around 1.3% accuracy drop. We validate the performance of Q3R for low-rank fine-tuning with experiments fine-tuning RoBERTa and Llama3 on GLUE tasks, for which Q3R achieves comparable performance compared to dense fine-tuning and state-of-the-art low-rank PEFT methods. Compared to state-of-the-art low-rank training methods such as LoRA [HS⁺19], LoRITa [AZW24], Q3R consistently produces models with better generalization at high truncation levels, without requiring overparameterization or full-rank warmup phases.

In Section 4, we elaborate the methodology of the proposed work, which is further discussed with a detailed derivation in the Supplementary material in Section A. In Section 5, we demonstrate the performance of Q3R, in comparison to other state-of-the-art methods. We continue with more experimental evaluations in the Supplementary material in Section D. Section D also includes discussions of the computational aspects of our methodology. In Section E, we demonstrate the robustness of Q3R to different hyperparameter variations. We briefly discuss the limitations of our work in Section 6.

3 Related Work

Parameter-Efficient Fine-Tuning (PEFT) Parameter-efficient fine-tuning is the concept of modifying only parts of a fully parametrized pretrained model to excel at a specific task of interest. PEFT methods such as adapters [HG⁺19] and LoRA [HS⁺19] introduce small, trainable modules into a frozen pretrained model, drastically reducing the number of parameters to be updated. These techniques often match full fine-tuning performance with only a tiny fraction of trainable parameters. However, the low-rank constraints that make LoRA-style methods efficient for downstream tasks also limit capacity if applied during pre-training. Training from scratch with only low-rank

adapters or factorizations (instead of full-rank weight updates) tends to underperform, as it restricts optimization to a low-dimensional subspace [ZZC⁺24]. LoRA assumes a well-formed pretrained weight W plus a low-rank perturbation of rank- r adapter matrices $A \in \mathbb{R}^{d \times r}$ and $B \in \mathbb{R}^{r \times d}$ such that $\Delta W = AB$; without a strong initial W , such updates struggle to capture the full complexity needed for learning from scratch. *KronA* replaces LoRA’s product with a Kronecker factorization for better rank-parameter trade-offs [ETK⁺25]. *DoRA* decouples update magnitude and direction via a learnable scaling factor, improving upon LoRA’s expressivity [LW⁺24]. *Compacter* uses shared, low-rank, Kronecker-parameterized adapters across layers, matching standard adapters with only 0.05 % extra parameters [MHR21].

Low-Rank Training in Neural Networks. Neural network training often exhibits implicit low-rank structure during training, as optimization dynamics like SGD with weight decay tend to bias models toward low-rank solutions [GSGP25, HMZ⁺23]. This observation has motivated a range of explicit low-rank training methods that constrain parameter matrices directly. A common approach factorizes weights and trains the factorized weights instead, reducing compute and memory costs with minor accuracy loss [KTMF21]. Techniques like LoRA [WMPG24] and its extensions [LS⁺23] inject low-rank updates into pretrained Transformer weights, enabling parameter-efficient adaptation. However, pre-training directly under low-rank constraints remains more challenging. [WMP⁺24] shares a similar motivation to ours—studying the limitations of LoRA-style low-rank pre-training and proposing an alternative regularization-driven approach to induce low-rank structure during training. Although we approach the problem through a different optimization framework, their analysis and framing of the limitations of adapter-based methods are highly relevant and can guide refinement of both the positioning and justification of our method. Regularization-based approaches use nuclear norm or log-determinant surrogates to promote low-rank solutions [SZ⁺23], while others apply orthogonality constraints and adaptive rank pruning [YYT⁺20, YCS⁺20]. In Transformers, low-rank parameterizations have achieved 2–5 \times compression with minimal performance drop [AZW24], and Cuttlefish [WAUC⁺23] automates rank selection by monitoring stable ranks during a warmup phase. Still, many methods rely on post-hoc truncation or overparameterization, which do not minimize rank during training. Our work addresses this gap by directly optimizing for low-rank solutions via reweighted least squares, promoting compact representations throughout pre-training. However, many of these methods rely on overparameterization or post-hoc truncation and do not directly minimize rank during training. In contrast, our approach promotes low-rank structure directly via optimization, using a principled regularization technique rooted in reweighted least squares.

Spectral Low-Rank Regularization. A related line of work studies algorithms that impose low-rankness of neural network matrices based on the nuclear norm, Schatten- p quasi-norm or a direct rank regularization. In particular, [AS17] proposed a proximal stochastic gradient descent applied to the nuclear norm. Methods that apply spectral truncation (e.g., via truncated SVD) during training or post-training [YT⁺20, XL⁺20] can also be understood within this framework. A downside of such approaches is the computational overhead: they require at least a truncated SVD at *every* iteration, which quickly becomes computationally prohibitive for larger networks. Moreover, arguably, such aggressive, discontinuous rank regularization interferes with the continuous gradient-based training process of the network.

In contrast, our proposed Q3R regularizer imposes low-rankness more *gradually* by reweighting at periodic intervals, at which a smoothing parameter is updated as well, which we find to be sufficient for convergence while significantly reducing the computational overhead. This “soft” imposition of low-rank structure aligns with insights from IRLS-based methods (see below). A spectral, Schatten- p regularization is also the core of the motivation of LoRITa [AZW24]; however, in this case, the spectral regularization can be seen as a justification of an (unweighted) squared Frobenius norm regularization on factor matrices, whereas Q3R does not work with factor matrices and considers a *reweighted* quadratic term.

Rank Regularization and IRLS. In a line of work that significantly precedes the interest in low-rank techniques for deep learning, the problem of identifying or learning a low-rank matrix from noisy, under-determined linear measurements has been studied for decades in control theory [FHB03, DCM22], recommender systems [Kor09, KBV09] and compressed sensing [RFP10, DR16]. Even in this setting, which is fundamentally linear unlike the training of deep neural networks, the minimization of a rank objective subject to the constraints is NP-hard [Nat95, RFP10], motivating

surrogate formulations or relaxations. Convex relaxations using the nuclear norm [CR09, RFP10, DR16, CW18] have been popular for a long time due to their strong recovery guarantees under suitable assumptions and their ability to be tackled using the machinery of convex optimization [BV04], but fail to result in a convex formulation in the deep learning setting. Even disregarding computational limitations of convex regularizations [CC18], *non-convex* rank surrogates such as the log-determinant penalty [FHB03] lead to algorithms which are more data-efficient, as evidenced for a variety of low-rank matrix recovery problems [FHB04, CESV13, KS18, KM23].

If combined with a suitable smoothing strategy, the non-smooth optimization framework of Iteratively Reweighted Least Squares (IRLS), originally pioneered by Weiszfeld [Wei37, WP09, BS15], has emerged as a leading algorithmic framework to optimize non-convex rank surrogates [FRW11, MF10, KMV21, GTK24] as it provides good trade-offs between scalability, data-efficiency, saddle-point evasion (present due to inherent non-convexity) and fast convergence. On a high level, IRLS solves a sequence of weighted Frobenius-norm problems that progressively suppress smaller singular values. The proposed rank regularization term Q3R (detailed in Section 4.1) builds on recent improvements on low-rank IRLS weight operator formulations [KMV21, GTK24] (or reweighting strategies), which, unlike older formulations [FRW11, MF10], allow for fast saddle-point evasion and locally quadratic convergence rates. To the best of our knowledge, IRLS-type low-rank regularization, which is at the core of Q3R, has not been explored in the literature in the context of deep learning so far. While providing an interesting perspective on older IRLS formulations [FRW11, MF10] from an *average gradient outer product* perspective, the recent work [RBD25] does not provide insights towards the derivation of quadratically convergent IRLS methods [KMV21, GTK24], nor does it extend the framework towards low-rank training of deep networks.

In the language of the low-rank recovery literature, LoRA-type [HS⁺19] approaches are known under the name of (*Burer-Monteiro* [BM03]) matrix factorization methods [SL16, ZL15, MWCC20, CLC19, ZCZ22, XS⁺23, SZ25]. While popular in applications [KBV09, RKZK22] due to their scalability, it is known that they can be outperformed by IRLS or Riemannian optimization approaches in more challenging setups involving, e.g., limited data [ZN22, LHLZ24], which is one motivation of our work.

4 Methodology

In this section, we provide a detailed derivation and definition of the *Quadratic Reweighted Rank Regularizer* Q3R in Section 4.1, before we embed it into a training scheme to train low-rank weights of deep learning models in Section 4.2.

4.1 Low-Rank Regularization via Q3R

Given a neural network with K weight matrices $\Theta = \{\mathbf{W}_i : \mathbf{W}_i \text{ is weight matrix, } i = 1, \dots, K\}$, a functionally ideal regularization term to add to the loss function of the network for the promotion of a low-rank weight is simply the *rank* of \mathbf{W} . However, $\text{rank}(\mathbf{W})$ is non-convex and not continuous, and thus hard to incorporate into a gradient-based training methodology.

In the following, we consider the *non-convex*, but continuously differentiable rank surrogate $F_\epsilon(\cdot)$ called ϵ -smoothed log-determinant, defined as

$$F_\epsilon(\mathbf{W}) := \sum_{i=1}^d f_\epsilon(\sigma_i(\mathbf{W})), \text{ where } f_\epsilon(\sigma) = \begin{cases} \epsilon^2 (\log(\sigma) - \log(\epsilon)) + \frac{1}{2}\epsilon^2, & \text{if } \sigma \geq \epsilon, \\ \frac{1}{2}\sigma^2, & \text{if } \sigma < \epsilon, \end{cases} \quad (1)$$

where $\sigma_i(\mathbf{W})$ is the i -th singular value of \mathbf{W} , and which is parameterized by a smoothing parameter $\epsilon > 0$. The definition of (1) follows [KM23] and is related to the log-determinant heuristics $\log \det(\mathbf{W} + \epsilon I) = \sum_{i=1}^d \log(\sigma_i(\mathbf{W}) + \epsilon)$ defined for positive semi-definite matrices $\mathbf{W} \in \mathbb{R}^{d \times d}$ of [FHB03, CESV13, RBD25]. Compared to other log-determinant type functions, $F_\epsilon(\cdot)$ from (1) has a few advantages: It is lower bounded by 0 for any ϵ and has a 1-Lipschitz gradient, making the objective compatible with gradient-based optimizers without extensive step-size adaptation. Furthermore, its smoothing parameter ϵ *regulates* the non-convexity of its optimization landscape and recovers the well-known squared Frobenius norm as $F_\epsilon(\mathbf{W}) = \frac{1}{2}\|\mathbf{W}\|_F^2$ in the case of $\sigma_1(\mathbf{W}) < \epsilon$.

The rank regularizer we study in this paper, however, is not simply $F_\epsilon(\cdot)$: If we were to work directly with the ϵ -smoothed log-determinant, its gradients $\nabla F_\epsilon(\mathbf{W})$ would require a full spectral decomposition of \mathbf{W} at each training iteration (see supplementary material).

Instead, we consider, given an expansion center point \mathbf{W}' (which may correspond to the current weight matrix during a neural network training dynamics), the *quadratic model* $Q_\epsilon(\cdot | \mathbf{W}')$ defined as

$$Q_\epsilon(\mathbf{W} | \mathbf{W}') = F_\epsilon(\mathbf{W}') + \frac{1}{2} \langle \mathbf{W}, \mathcal{R}_{\mathbf{W}', \epsilon}(\mathbf{W}) \rangle - \frac{1}{2} \langle \mathbf{W}', \mathcal{R}_{\mathbf{W}', \epsilon}(\mathbf{W}') \rangle, \quad (2)$$

where $\mathcal{R}_{\mathbf{W}', \epsilon}(\cdot) : \mathbb{R}^{d_1 \times d_2} \rightarrow \mathbb{R}^{d_1 \times d_2}$ is a positive definite, so-called *reweighting operator* [KMV21, GTK24], defined in Definition 4.1 below.

Definition 4.1 (Reweighting Operator [KM23]). *Let $\epsilon > 0$ and $\mathbf{W}' \in \mathbb{R}^{d_1 \times d_2}$ be a matrix with singular value decomposition $\mathbf{W}' = \mathbf{U}_{\mathbf{W}'} \text{diag}(\sigma_i(\mathbf{W}')) \mathbf{V}_{\mathbf{W}'}^\top$, where $\mathbf{U} \in \mathbb{R}^{d_1 \times r(\mathbf{W}', \epsilon)}$ and $\mathbf{V} \in \mathbb{R}^{d_2 \times r(\mathbf{W}', \epsilon)}$ are matrices of the leading $r(\mathbf{W}', \epsilon)$ left and right singular vectors satisfying $\mathbf{U}_{\mathbf{W}'} = [\mathbf{U} \quad \mathbf{U}_\perp] \in \mathbb{R}^{d_1 \times d_1}$ and $\mathbf{V}_{\mathbf{W}'} = [\mathbf{V} \quad \mathbf{V}_\perp] \in \mathbb{R}^{d_2 \times d_2}$, and*

$$r(\mathbf{W}', \epsilon) := |\{i \in \{1, \dots, \min(d_1, d_2)\} : \sigma_i(\mathbf{W}') > \epsilon\}| \quad (3)$$

is the number of singular values of \mathbf{W}' larger than ϵ . Then we define the reweighting operator $\mathcal{R}_{\mathbf{W}', \epsilon} : \mathbb{R}^{d_1 \times d_2} \rightarrow \mathbb{R}^{d_1 \times d_2}$ associated to the matrix \mathbf{W}' and smoothing parameter ϵ as

$$\mathcal{R}_{\mathbf{W}', \epsilon}(\mathbf{W}) = \mathbf{U}_{\mathbf{W}'} \Sigma_{\epsilon, d_1}^{-1} \mathbf{U}_{\mathbf{W}'}^\top \mathbf{W} \mathbf{V}_{\mathbf{W}'} \Sigma_{\epsilon, d_2}^{-1} \mathbf{V}_{\mathbf{W}'}^\top,$$

where $\Sigma_{\epsilon, d} = \text{diag}(\max(\sigma_i(\mathbf{W}')/\epsilon, 1))_{i=1}^d \in \mathbb{R}^{d \times d}$ for $d \in \{d_1, d_2\}$.

The reweighting operator satisfies the following simple properties (shown in the supplementary material), which makes working with it computationally feasible.

Lemma 4.1. *For $\epsilon > 0$ and \mathbf{W}' , let $\mathbf{U} \in \mathbb{R}^{d_1 \times r(\mathbf{W}', \epsilon)}$, $\mathbf{V} \in \mathbb{R}^{d_2 \times r(\mathbf{W}', \epsilon)}$ and $\mathcal{R}_{\mathbf{W}', \epsilon} : \mathbb{R}^{d_1 \times d_2} \rightarrow \mathbb{R}^{d_1 \times d_2}$ be as in Definition 4.1. Then the following statements are true:*

1. $\mathcal{R}_{\mathbf{W}', \epsilon}(\cdot)$ is a positive definite operator with respect to the Frobenius inner product $\langle \mathbf{A}, \mathbf{B} \rangle = \text{tr}(\mathbf{A}^\top \mathbf{B})$, i.e., $\langle \mathbf{W}, \mathcal{R}_{\mathbf{W}', \epsilon}(\mathbf{W}) \rangle > 0$ for all non-zero $\mathbf{W} \in \mathbb{R}^{d_1 \times d_2}$.

2. The image $\mathcal{R}_{\mathbf{W}', \epsilon}(\mathbf{W})$ of any $\mathbf{W} \in \mathbb{R}^{d_1 \times d_2}$ w.r.t. the reweighting operator can be computed as

$$\begin{aligned} \mathcal{R}_{\mathbf{W}', \epsilon}(\mathbf{W}) &= \epsilon^2 \mathbf{U} \Sigma^{-1} \mathbf{U}^\top \mathbf{W} \mathbf{V} \Sigma^{-1} \mathbf{V}^\top + \epsilon \mathbf{U} \Sigma^{-1} \mathbf{U}^\top \mathbf{W} (\mathbf{I} - \mathbf{V} \mathbf{V}^\top) \\ &\quad + \epsilon (\mathbf{I} - \mathbf{U} \mathbf{U}^\top) \mathbf{W} \mathbf{V} \Sigma^{-1} \mathbf{V}^\top + (\mathbf{I} - \mathbf{U} \mathbf{U}^\top) \mathbf{W} (\mathbf{I} - \mathbf{V} \mathbf{V}^\top), \end{aligned} \quad (4)$$

where $\Sigma = \text{diag}(\sigma_i(\mathbf{W}'))_{i=1}^{r(\mathbf{W}', \epsilon)} \in \mathbb{R}^{r(\mathbf{W}', \epsilon) \times r(\mathbf{W}', \epsilon)}$ is the diagonal matrix containing the largest $r(\mathbf{W}', \epsilon)$ singular values of \mathbf{W}' .

3. The quadratic model of (2) satisfies, for all $\mathbf{W}, \mathbf{W}' \in \mathbb{R}^{d_1 \times d_2}$, that

$$Q_\epsilon(\mathbf{W} | \mathbf{W}') = F_\epsilon(\mathbf{W}') + \langle \nabla F_\epsilon(\mathbf{W}'), \mathbf{W} - \mathbf{W}' \rangle + \frac{1}{2} \langle \mathbf{W} - \mathbf{W}', \mathcal{R}_{\mathbf{W}', \epsilon}(\mathbf{W} - \mathbf{W}') \rangle. \quad (5)$$

We note that the quadratic model $Q_\epsilon(\cdot | \mathbf{W}')$ (2) defined by $\mathcal{R}_{\mathbf{W}', \epsilon}$ is a *majorizing* quadratic model that satisfies $Q_\epsilon(\mathbf{W} | \mathbf{W}') \geq F_\epsilon(\mathbf{W})$ for all $\mathbf{W} \in \mathbb{R}^{d_1 \times d_2}$.² It is *different* from a second-order Taylor expansion of the $F_\epsilon(\cdot)$ about \mathbf{W}' , which would only be an *approximation*, but no *majorization* due to the non-convex nature of $F_\epsilon(\cdot)$. The quadratic model can still be related to a second-order Taylor expansion of F_ϵ via (5) as each generalized Hessian [HUSN84] $\partial^2 F_\epsilon(\mathbf{W}')$ of F_ϵ satisfies $\partial^2 F_\epsilon(\mathbf{W}') \leq \mathcal{R}_{\mathbf{W}', \epsilon}$ in the Loewner order.

We observe that in the quadratic model $Q_\epsilon(\mathbf{W} | \mathbf{W}')$ of (2), the only term that depends on \mathbf{W} is the second summand. Thus, to obtain a simple, *differentiable* regularizer term that can be incorporated into a deep learning framework, we define the *Quadratic Reweighted Rank Regularizer* Q3R of a neural network weight matrix $\mathbf{W} \in \mathbb{R}^{d_1 \times d_2}$, given $\mathbf{W}' \in \mathbb{R}^{d_1 \times d_2}$ and $\epsilon > 0$, as $\text{Q3R}_{\mathbf{W}', \epsilon} : \mathbb{R}^{d_1 \times d_2} \rightarrow \mathbb{R}$ with

$$\text{Q3R}_{\mathbf{W}', \epsilon}(\mathbf{W}) = \frac{1}{2} \langle \mathbf{W}, \mathcal{R}_{\mathbf{W}', \epsilon}(\mathbf{W}) \rangle. \quad (6)$$

As we see in the next section, it is simple and tractable to compute its gradient $\nabla_{\mathbf{W}} \text{Q3R}_{\mathbf{W}', \epsilon}(\mathbf{W}) \in \mathbb{R}^{d_1 \times d_2}$, which can be used by any gradient-based optimizer.

²This majorization property is implicitly postulated in [KMV21, KM23], but without proof. While proving this property is beyond the scope of this paper, we believe that the statement is true.

Algorithm 1 Update Reweighting Operator $\mathcal{R}_{\mathbf{W}', \epsilon_{\text{old}}}(\cdot) \mapsto \mathcal{R}_{\mathbf{W}, \epsilon_{\text{new}}}(\cdot)$

Input: NN weight matrix $\mathbf{W} \in \mathbb{R}^{d_1 \times d_2}$; target rank r_{target} ; prev. smoothing parameter ϵ_{old} .
Output: Updated ϵ_{new} , reweighting operator $\mathcal{R}_{\mathbf{W}, \epsilon_{\text{new}}}$ (via $\Sigma, \mathbf{U}, \mathbf{V}$), envelope rank r_{env}

- 1: Compute $[\mathbf{U}, \Sigma, \mathbf{V}] = \text{SVD}^{\epsilon_{\text{old}}}(\mathbf{W})$ of \mathbf{W} , where $\text{SVD}^{\epsilon_{\text{old}}}(\cdot)$ computes a partial singular value decomposition of its input up to order $r(\cdot, \epsilon_{\text{old}})$ (see (3)) as well as $\sigma_{r_{\text{target}}+1}(\mathbf{W})$.
- 2: $\epsilon_{\text{new}} = \min(\epsilon_{\text{old}}, \sigma_{r_{\text{target}}+1}(\mathbf{W}))$. \triangleright UPDATE SMOOTHING (7)
- 3: $r_{\text{env}} = r(\mathbf{W}, \epsilon_{\text{new}})$. \triangleright UPDATE RANK ENVELOPE
- 4: Set $\mathbf{U} = \mathbf{U}_{:, 1:r_{\text{env}}}$, $\mathbf{V} = \mathbf{V}_{:, 1:r_{\text{env}}}$, $\Sigma = \Sigma_{1:r_{\text{env}}, 1:r_{\text{env}}}$ \triangleright RESTRICT PART. SVD MATRICES
- 5: **return** Reweighting operator $\mathcal{R}_{\mathbf{W}, \epsilon_{\text{new}}}$ implicitly defined by $\mathbf{U} \in \mathbb{R}^{d_1 \times r_{\text{env}}}$, $\mathbf{V} \in \mathbb{R}^{d_2 \times r_{\text{env}}}$, $\Sigma \in \mathbb{R}^{r_{\text{env}} \times r_{\text{env}}}$ & ϵ_{new} .

Furthermore, we periodically (but not at each training iteration) *update* the reweighting operator of Q3R (and thus, the underlying quadratic model $Q_{\epsilon}(\mathbf{W} | \mathbf{W}')$) by setting $\mathbf{W}' \leftarrow \mathbf{W}$ and re-compute $\mathcal{R}_{\mathbf{W}', \epsilon}$, for which a truncated SVD of \mathbf{W} is sufficient due to (4). Additionally, whenever updating $\mathcal{R}_{\mathbf{W}', \epsilon}$, we apply the *non-increasing* update

$$\epsilon \leftarrow \min(\epsilon, \sigma_{r_{\text{target}}+1}(\mathbf{W})) \quad (7)$$

to the smoothing parameter ϵ , which uses a *target rank* parameter r_{target} as an input. The rationale of this smoothing parameter update is two-fold: first, this choice gives *partial control* on the expected rank of the weight matrix after training, as the value of $\mathcal{R}_{\mathbf{W}', \epsilon}(\mathbf{W})$ tends to 0 if ϵ follows the dynamics of (7) in the case of $\epsilon \rightarrow 0$ for matrices \mathbf{W} whose row and column spaces are both orthogonal to the columns of \mathbf{U} and \mathbf{V} , respectively. Second, this choice increases the *non-convexity* the ϵ -smoothed log-determinant F_{ϵ} underlying Q3R *gradually* [YATC20], facilitating a fast convergence to true low-rank solutions without becoming trapped in high-rank local minima [KMW21, KM23]. We summarize computational steps of a reweighting operator update in Algorithm 1.

4.2 Neural Network Training via AdamQ3R

Let now $y : \mathbb{R}^{d_1^1 \times d_2^1} \times \mathbb{R}^{d_1^K \times d_2^K} \times \mathbb{R}^{d_{\text{in}}} \rightarrow \mathbb{R}^{d_{\text{out}}}$ be the input-output mapping of a deep neural network that depends on weight parameter matrices $\Theta = \{\mathbf{W}_k \in \mathbb{R}^{d_1^k \times d_2^k} : \mathbf{W}_k \text{ is weight matrix, } k = 1, \dots, K\}$. For a Transformer-based architecture such as Vision Transformer [DBK21], the weight matrices include square layer- and head-wise query, key and value weight matrices $\mathbf{W}_q, \mathbf{W}_k, \mathbf{W}_v \in \mathbb{R}^{d \times d}$ as well as rectangular projection and MLP layer weight matrices. Given a pairwise loss $\ell(\cdot, \cdot)$ such as cross entropy and a training dataset $\{x_i, y_i\}_{i=1}^n$, we can define the (unregularized) network loss as $\mathcal{L}(\Theta) = \frac{1}{n} \sum_{i=1}^n \ell(y(\Theta, x_i), y_i)$.

In order to gradually impose low-rank weights during training, we propose to optimize instead the Q3R-regularized total loss

$$\mathcal{L}_{\text{Q3R}}(\Theta) := \mathcal{L}(\Theta) + \lambda \sum_{\substack{k=1 \\ \text{Q3R is active for } \mathbf{W}_k}}^K \text{Q3R}_{\mathbf{W}'_k, \epsilon_k}(\mathbf{W}_k) \quad (8)$$

where $\lambda > 0$ is a regularization parameter and the $\text{Q3R}_{\mathbf{W}'_k, \epsilon_k}(\cdot)$ are as in (6); the $\{\mathbf{W}'_k\}$ are initially set to the initialization weights, and $\epsilon_k = \infty$ for each $k = 1, \dots, K$. We observe that due to the definition of Q3R, the gradient with respect to the regularizer terms can be computed as $\nabla_{\mathbf{W}_k} \text{Q3R}_{\mathbf{W}'_k, \epsilon_k}(\mathbf{W}_k) = \mathcal{R}_{\mathbf{W}'_k, \epsilon_k}(\mathbf{W}_k)$ for each k , i.e., by computing the image of \mathbf{W}_k with respect to the reweighting operator $\mathcal{R}_{\mathbf{W}'_k, \epsilon_k}(\cdot)$ of Definition 4.1.

The Q3R-regularized loss \mathcal{L}_{Q3R} can now be used in conjunction with any optimizer suitable for

Algorithm 2 Low-Rank Training via AdamQ3R

Input: Minibatch size B , reweighting period T , Q3R parameter λ , learning rate $\alpha = 0.001$, $\beta_1 = 0.9$, $\beta_2 = 0.999$, $\delta = 10^{-8}$, $\eta = 3$, target rank r_{target} .

- 1: Initialize parameter \mathbf{W}_0, ϵ_0 and reweighting operator $\mathcal{R}_{\mathbf{W}_0, \epsilon_0}$.
- 2: **for** $t = 0, 1, \dots$ **do**
- 3: **if** $t \bmod T = 0$ **then**
- 4: Update reweighting operator $\mathcal{R}_{\lfloor \frac{t}{T} \rfloor}(\cdot) := \mathcal{R}_{\mathbf{W}_t, \epsilon_t}(\cdot)$ and ϵ_t \triangleright USE ALGORITHM 1
- 5: **end if**
- 6: Sample minibatch $S = \{(x_i, y_i)\}_{i=1}^B$
- 7: $\mathbf{g}_{t+1} \leftarrow \nabla_{\mathbf{W}} \mathcal{L}_S(\mathbf{W}_t)$ \triangleright COMPUTE BATCH GRADIENT OF \mathcal{L}
- 8: $\mathbf{m}_{t+1} \leftarrow \beta_1 \mathbf{m}_t + (1 - \beta_1) \mathbf{g}_{t+1}$
- 9: $\mathbf{v}_{t+1} \leftarrow \beta_2 \mathbf{v}_t + (1 - \beta_2) \mathbf{g}_{t+1}^2$
- 10: $\hat{\mathbf{m}}_{t+1} \leftarrow \mathbf{m}_{t+1} / (1 - \beta_1^{t+1})$
- 11: $\hat{\mathbf{v}}_{t+1} \leftarrow \mathbf{v}_{t+1} / (1 - \beta_2^{t+1})$
- 12: $\mathbf{R}_t \leftarrow \mathcal{R}_{\lfloor \frac{t}{T} \rfloor}(\mathbf{W}_t)$ \triangleright COMPUTE Q3R GRADIENT (4)
- 13: $\mathbf{W}_{t+1} \leftarrow \mathbf{W}_t - \eta \left(\frac{\alpha \hat{\mathbf{m}}_{t+1}}{\sqrt{\hat{\mathbf{v}}_{t+1}} + \delta} + \lambda \mathbf{R}_t \right)$
- 14: **end for**
- 15: **return** \mathbf{W}_t

the neural network architecture such as minibatch stochastic gradient or Adam [KB15]. To ensure that the quadratic models underlying Q3R match the ϵ_k -smoothed log-determinant rank surrogates $F_{\epsilon_k}(\cdot)$ closely, we update the reweighting operators $\mathcal{R}_{\mathbf{W}'_{k^*, \epsilon_k}}(\cdot)$ via Algorithm 1 on a fixed iteration schedule of every T training iterations—we call this parameter T the *reweighting period*.

However, instead of using a generic adaptive gradient optimizer such as Adam on \mathcal{L}_{Q3R} , we observe that the Q3R terms already possess accurate second-order information of underlying regularization surrogate, which means that including the Q3R terms into the adaptive part of an Adam-like optimizer is likely to be suboptimal. For this reason, we propose to use a dedicated adaptive optimizer to optimize \mathcal{L}_{Q3R} , dubbed *AdamQ3R*, which is detailed in Algorithm 2. AdamQ3R extends the observation of AdamW [LH19] that a decoupling of regularization term (in that case, squared Frobenius norm regularization) and network loss improves generalization performance to Q3R regularization, avoiding a distortion of the loss landscape. A validation of the benefits of using AdamQ3R vs. standard Adam applied to \mathcal{L}_{Q3R} can be found in the supplementary material.

Computational Aspects. Following the low-rank training framework of Q3R, for example, via AdamQ3R, introduces a limited computational overhead compared to unregularized deep learning. Every T training iterations, a truncated singular value decomposition of order r_{env} (see Algorithm 1) of each weight matrix $\mathbf{W}_i \in \mathbb{R}^{d_1 \times d_2}$ to which Q3R is applied is required, which has a time complexity of $O(d_1 d_2 r_{\text{env}} + (d_1 + d_2) r_{\text{env}}^2)$ [HMT11]. Similarly, calculating a Q3R gradient \mathbf{R}_t in Algorithm 2 imposes a total cost of $O(d_1 d_2 r_{\text{env}} + (d_1 + d_2) r_{\text{env}}^2 + r_{\text{env}}^3)$. Since the smoothing parameter update rule (7) is designed to relate r_{env} with the target rank r_{target} such that $r_{\text{env}} \approx r_{\text{target}}$, the additional time complexity is somewhat proportional to the target rank. To obtain significant parameter reductions in the trained network weight matrices, it is chosen such that $r_{\text{target}} \ll \min(d_1, d_2)$, which limits the computational overhead of Q3R in the most interesting use cases. Additional memory requirements amount to $r_{\text{env}}(d_1 + d_2 + 1)$ per weight matrix as the reweighting operator information needs to be stored via \mathbf{U} , \mathbf{V} and Σ .

5 Experiments

We explore the ability of Q3R to obtain favorable trade-offs between model performance and parameter-efficiency across diverse architectures and data distributions experimentally. To this end, we compare different low-rank training methodologies across a range of architecture-dataset pairs: we pre-train ViT-Tiny [DBK21, SKZ⁺22] on CIFAR-10, ViT-Base [DBK21] on CIFAR-100, followed by post-training low-rank truncation [AZW24]; further, we fine-tune BERT-Large [DC⁺19] on GLUE benchmark tasks (without truncation).

5.1 Low-Rank Pre-Training

We compare the accuracy of models trained by Q3R against baselines LoRiT_a [AZW24], LoRA [HS⁺19], and a model trained without low-rank regularization, after post-training truncation. After training, we truncate each layer weight matrix $\mathbf{W}_k \in \Theta$ using a truncated SVD to obtain factor matrices \mathbf{A}, \mathbf{B} with inner dimension r and $\mathbf{W}_k \approx \mathbf{A}\mathbf{B}$ for a range of ranks r corresponding to different parameter retention percentages p . Depending on the experiment, we apply low-rank regularization to different subsets of weights $\{\mathbf{W}_k\}$.

ViT-Tiny Trained on CIFAR-10. We train ViT-Tiny on CIFAR-10 for 100 epochs using a learning rate of $\alpha = 0.00004$. We enable low-rank training for all Transformer blocks, accounting for 96% of ViT-Tiny’s parameters. We conduct a hyperparameter sweep across different configurations, and Figure 1a shows the best performance achieved by each training method when rank regularization is applied to the MLP and QKV weights. From Table 1, we find that AdamQ3R retains 42.4% of the original parameters with only a 1.22% performance drop, and retains 23.2% of parameters with a 4.4% performance drop, while LoRiT_a consistently underperforms in comparison. As shown in Figure 1b, despite various hyperparameter configurations λ and d for LoRiT_a, AdamQ3R consistently outperforms LoRiT_a upon truncation.

Model\Parameter Retention p	5%	10%	15%	20%	30%	40%	100%
Vanilla ViT-T	0.1475	0.1252	0.1350	0.1213	0.1624	0.1524	0.6840
LoRA	-	0.3546	0.3655	0.3576	-	-	-
LoRITa D=2, $\lambda=10^{-1}$	0.0989	0.1433	0.1543	0.2125	0.3247	0.4523	0.7142
LoRITa D=3, $\lambda=10^{-1}$	0.2258	0.3861	0.4466	0.5035	0.6368	0.6740	0.7273
LoRITa D=3, $\lambda=10^{-3}$	0.1338	0.2136	0.3839	0.4560	0.5973	0.6253	0.7449
Q3R, $r_{\text{target}} = 10\%$, $\lambda=10^{-3}$	0.2322	0.4085	0.5606	0.6295	0.6526	0.6654	0.6843
Q3R, $r_{\text{target}} = 15\%$, $\lambda=10^{-3}$	0.1796	0.4758	0.5883	0.6215	0.6455	0.6555	0.6737
Q3R, $r_{\text{target}} = 20\%$, $\lambda=10^{-3}$	0.1998	0.4737	0.6175	0.6511	0.6749	0.6833	0.6990
Q3R, $r_{\text{target}} = 10\%$, $\lambda=10^{-2}$	0.2041	0.4387	0.6115	0.6449	0.6707	0.6771	0.6889
Q3R, $r_{\text{target}} = 15\%$, $\lambda=10^{-2}$	0.1313	0.3896	0.6158	0.6550	0.6689	0.6801	0.6982
Q3R, $r_{\text{target}} = 20\%$, $\lambda=10^{-2}$	0.1870	0.4335	0.6123	0.6496	0.6744	0.6868	0.6962

Table 1: MLP truncation performance of ViT-T, rank regularization is applied to *both* attention (QKV) blocks and MLP blocks. For LoRA, factor ranks are adaptive to p .

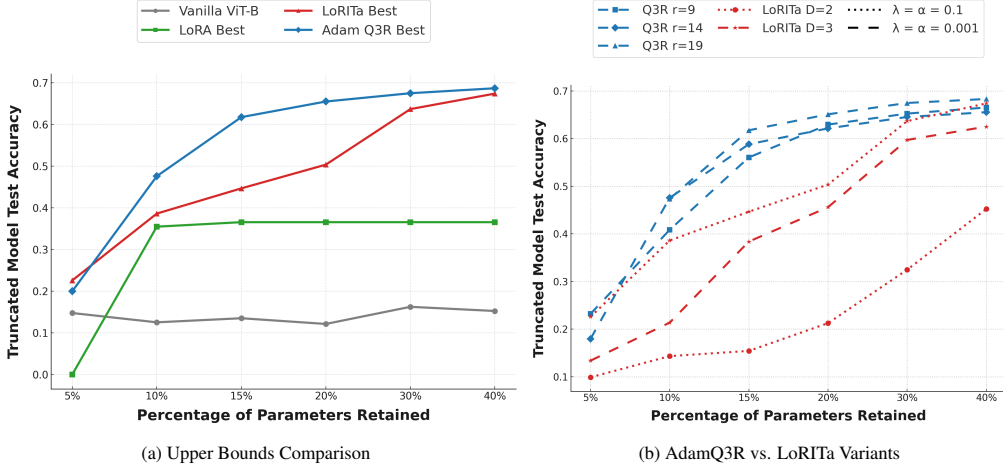


Figure 1: Performance curves on CIFAR-10 with rank regularization applied to MLP and QKV blocks: (a) Best performance across methods, (b) AdamQ3R vs. LoRITa variants.

ViT-Base Trained on CIFAR-100. To demonstrate the performance of the low-rank pre-training methods on a more challenging dataset and larger model, we train the 86M parameter ViT-Base from scratch for 100 epochs on CIFAR-100 with data augmentation and $\alpha = 0.0001$ [SKZ⁺22]. In line with practice for large-scale Transformers [LFX⁺24], we apply low-rank training techniques solely to the multi-head self-attention blocks (QKV, but not to the MLP blocks). Despite the additional size and complexity of ViT-Base compared to ViT-Tiny, Q3R remains robust and we see in Figures 2a and 2b that it exhibits larger performance advantages with 0.40-0.44 test accuracy when 20% parameters retained, whereas LoRITa models do not exceed an accuracy of 0.25 at the same truncation level despite their substantial overparameterization. Figures 2a and 2b are in reference to the Table 6 in the supplementary material.

ViT-Tiny with Low-Rank Attention Weights. We train ViT-Tiny for 100 epochs on CIFAR-10 [Kri09] from scratch with learning rate $\alpha = 0.0004$, with low-rank regularization applied only to attention weights. We evaluate the methods for a larger set of hyperparameters as shown in Figure 3b using layer-wise truncation levels with retained parameter percentages $p \in \{5\%, 10\%, 15\%, 20\%, 30\%, 40\%, 50\%, 60\%, 70\%, 80\%, 90\%\}$, and present results in Figure 3. Figure 3a shows that Q3R experiences almost no performance drop up to $p = 30\%$ for most parameter choices, exceeding the performance of reference methods. Figure 3b shows that the worst performing Q3R model still outperforms any LoRA, LoRITa, or vanilla ViT-Tiny below $p = 60\%$, showcasing the method’s robustness. Figures 3 and 3a are based on Table 5 in the supplementary material.

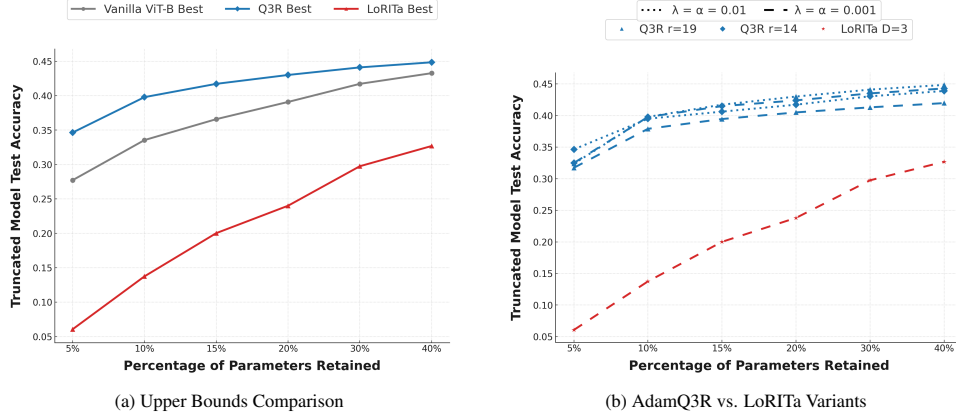


Figure 2: Performance curves on CIFAR-100 with rank regularization applied to QKV blocks: (a) Best performance across methods, (b) AdamQ3R vs. LoRITA variants.

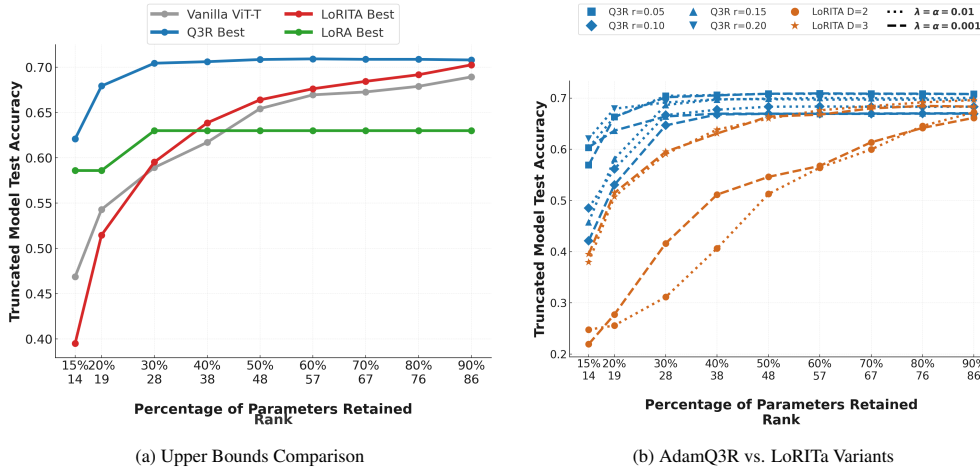


Figure 3: Performance curves on CIFAR-10 with rank regularization applied to QKV blocks: (a) Best performance across methods, (b) AdamQ3R vs. LoRITA variants.

ViT-Base on ImageNet-1k. We train ViT-Base on ImageNet-1k using Automatic Mixed Precision [MNA⁺18] with AutoAugmentation [CZ⁺19] for 100 epochs. Training is conducted with a learning rate of $\alpha = 4 \times 10^{-5}$, a batch size of 384, and gradient clipping [ZHSJ20] across 4 L40S GPUs. We observe that Q3R consistently outperforms the baseline model while utilizing fewer parameters. This performance advantage holds under two truncation paradigms: attention matrices only, and entire Transformer blocks. In both cases, Q3R maintains performance comparable to the full baseline model, as seen in Table 2.

Optimizer Transformer Modules	10%	15%	20%	30%	40%	50%	100%
AdamQ3R QKV, MLP	0.0138	0.1439	0.3376	0.421	0.4458	0.4556	0.5816
Adam QKV, MLP	0.0193	0.0976	0.2950	0.399	0.4311	0.4523	0.5179
AdamQ3R QKV	0.1713	0.3016	0.4623	0.4895	0.4952	0.4975	0.5816
Adam QKV	0.2552	0.3366	0.4551	0.4882	0.4882	0.4937	0.5179

Table 2: ViT-Base on ImageNet-1k validation accuracy post-truncation on the last epoch

5.2 Low-Rank Fine-Tuning

Q3R not only induces a low-rank structure during pre-training in a memory-efficient manner, but also extends naturally to compact fine-tuning. We fine-tune pretrained RoBERTa models on the GLUE benchmark using AdamQ3R with the proposed Q3R regularizer, and compare against full fine-tuning

Table 3: GLUE Benchmark Scores

Method	MRPC	RTE	CoLA	STS-B	SST-2	QQP	MNLI	QNLI	Average
Dense Fine-tuning	91.9	77.62	62.3	90.19	94.04	90.2	87.3	91.49	85.88
LoRA-4	89.04	73.55	56.25	89.86	94.3	90.11	87.00	92.5	84.58
Q3R-4	92.24	77.23	63.5	90.1	92.2	91.6	87.2	90.2	85.86

and LoRA [HS⁺19]. We impose Q3R on the weight matrices that are added to the full-rank pretrained weight matrices. For LoRA, we adopt the hyperparameters from [HS⁺19], and for Q3R we cross-validate the learning rate and regularization hyperparameter λ . As shown in Table 3, Q3R matches or exceeds LoRA’s accuracy on most tasks and exhibits a performance closer to dense fine-tuning. These results demonstrate that Q3R can serve as a unified, low-rank training strategy—both for pre-training and fine-tuning of Transformer models. We discuss additional fine-tuning experiments in Section D.2.

6 Limitations

While our experiments showcase a robust post-truncation accuracy of Q3R-trained Transformers on vision and natural language tasks in small-to-medium scale settings that exceeds (or in the case of fine-tuning, matches) the one of other relevant low-rank training paradigms, the viability of Q3R is yet to be established across diverse architectures and large-scale problems. Fundamentally, Q3R relies on a suitable choice of the regularization strength hyperparameter λ , as well as on a suitable choice of the target rank r_{target} . We provide ablations about these values in Section E.1. While Q3R exhibits vulnerability to elevated values of λ due to a convergence to a trivial, very low-rank matrix, this is easily detectable by monitoring the tail ratio $T(X, r) = \frac{\sum_{i=1}^r \sigma_i^2}{\|X\|_F^2}$ on models. In practice, we have observed stable behavior within the range $\lambda \in [0.001, 0.01]$. The target rank r_{target} remains insensitive to underestimation because of the direct computation of epsilon resulting in a large ϵ , and due to the monotonicity of the smoothing parameter update function (7), ϵ remains within a reasonable bound. We note that for weight matrices and iterations with large ϵ , the effect of AdamQ3R resembles the one of AdamW with weight decay parameter λ (see also (6)).

Arguably, a limitation of this work is also the fact that while the final weights after training are (for appropriate parameters) low-rank, AdamQ3R still handles *dense* weight matrix variables throughout training, which does not allow a reduction of the parameter budget *during* training, unlike recent work [MHP25]. More elaborate post-training post-processing (e.g., inspired by [WAUc⁺23]) might lead to further performance improvements.

7 Conclusion

We introduced *Quadratic Reweighted Rank Regularizer* (Q3R), a principled, optimizer-compatible framework for inducing low-rank structure in deep neural network weights through explicit, continuous regularization. By majorizing a smoothed log-determinant surrogate with a quadratic model embedded in the AdamQ3R optimizer, Q3R trains weight matrices to achieve target ranks with minimal accuracy loss. This enables model compression with negligible performance degradation under reasonable parameter reductions, decreasing deployment costs and increasing throughput. Our experimental results demonstrate that Q3R generalizes across modalities and training regimes, with its design being particularly suitable for low-rank pre-training. Reducing Q3R’s computational overhead, for example via low-rank subspace projections, remains to future work.

Acknowledgements

We would like to thank Tonmoy Hasan and Arkaprava Sinha for their assistance in setting up the LLM experiments. I.G. and C.K acknowledge the support of the NSF Grant CCF-2549926 for this work.

References

- [AS17] J. M. Alvarez and M. Salzmann. Compression-aware training of deep networks. In *Advances in Neural Information Processing Systems (NeurIPS)*, 2017.
- [AZW24] I. Alkhouri, X. Zhang, and R. Wang. Structure-Preserving Network Compression Via Low-Rank Induced Training Through Linear Layers Composition. *Transactions on Machine Learning Research*, 2024.
- [Bec17] A. Beck. *First-Order Methods in Optimization*. MOS-SIAM Ser. Optim, Philadelphia, PA, 2017.
- [BM03] S. Burer and R. D. Monteiro. A nonlinear programming algorithm for solving semidefinite programs via low-rank factorization. *Mathematical Programming*, 95(2):329–357, 2003.
- [BS15] A. Beck and S. Sabach. Weiszfeld’s Method: Old and New Results. *J. Optim. Theory Appl.*, 164(1):1–40, 2015.
- [BV04] S. P. Boyd and L. Vandenberghe. *Convex optimization*. Cambridge university press, 2004.
- [CC18] Y. Chen and Y. Chi. Harnessing Structures in Big Data via Guaranteed Low-Rank Matrix Estimation: Recent Theory and Fast Algorithms via Convex and Nonconvex Optimization. *IEEE Signal Process. Mag.*, 35(4):14–31, 2018.
- [CESV13] E. J. Candès, Y. Eldar, T. Strohmer, and V. Voroninski. Phase Retrieval via Matrix Completion. *SIAM J. Imag. Sci.*, 6(1):199–225, 2013.
- [CLC19] Y. Chi, Y. M. Lu, and Y. Chen. Nonconvex Optimization Meets Low-Rank Matrix Factorization: An Overview. *IEEE Trans. Signal Process.*, 67(20):5239–5269, 2019.
- [CR09] E. J. Candès and B. Recht. Exact matrix completion via convex optimization. *Found. Comput. Math.*, 9(6):717–772, 2009.
- [CW18] J.-F. Cai and K. Wei. Exploiting the Structure Effectively and Efficiently in Low-Rank Matrix Recovery. *Processing, Analyzing and Learning of Images, Shapes, and Forms*, 19:21 pp., 2018.
- [CZ⁺19] E. D. Cubuk, B. Zoph, et al. AutoAugment: Learning Augmentation Policies from Data. In *Conference on Computer Vision and Pattern Recognition (CVPR)*, 2019.
- [DBKea21] A. Dosovitskiy, L. Beyer, A. Kolesnikov, and et al. An Image is Worth 16x16 Words: Transformers for Image Recognition at Scale. In *International Conference on Learning Representations (ICLR)*, 2021.
- [DC⁺19] J. Devlin, M.-W. Chang, et al. BERT: Pre-training of Deep Bidirectional Transformers for Language Understanding. In *Proceedings of the 2019 Conference of the North American Chapter of the Association for Computational Linguistics: Human Language Technologies, Volume 1*, 2019.
- [DCM22] F. Dörfler, J. Coulson, and I. Markovsky. Bridging direct and indirect data-driven control formulations via regularizations and relaxations. *IEEE Transactions on Automatic Control*, 68(2):883–897, 2022.
- [DR16] M. A. Davenport and J. Romberg. An Overview of Low-Rank Matrix Recovery From Incomplete Observations. *IEEE J. Sel. Topics Signal Process.*, 10:608–622, 2016.
- [ETK⁺25] A. Edalati, M. Tahaei, I. Kobzyev, V. P. Nia, J. J. Clark, and M. Rezagholizadeh. KronA: Parameter-Efficient Tuning with Kronecker Adapter. In *Enhancing LLM Performance: Efficacy, Fine-Tuning, and Inference Techniques*. Springer, 2025.
- [FHB03] M. Fazel, H. Hindi, and S. P. Boyd. Log-det heuristic for matrix rank minimization with applications to Hankel and Euclidean distance matrices. In *Proceedings of the American Control Conference*, volume 3, pages 2156–2162, 2003.

- [FHB04] M. Fazel, H. Hindi, and S. Boyd. Rank minimization and applications in system theory. In *Proceedings of the 2004 American Control Conference*, 2004.
- [FRW11] M. Fornasier, H. Rauhut, and R. Ward. Low-rank Matrix Recovery via Iteratively Reweighted Least Squares Minimization. *SIAM J. Optim.*, 21(4):1614–1640, 2011.
- [GK⁺22] A. N. Gomez, S. R. Kamalakara, et al. Exploring Low Rank Training of Deep Neural Networks. *arXiv preprint arXiv:2209.13569*, 2022.
- [GSGP25] T. Galanti, Z. S. Siegel, A. Gupte, and T. A. Poggio. SGD with weight decay secretly minimizes the ranks of your neural networks. In *The Second Conference on Parsimony and Learning (CPAL 2025)*, 2025.
- [GTK24] I. Ghosh, A. Tasissa, and C. Kümmerle. Sample-Efficient Geometry Reconstruction from Euclidean Distances using Non-Convex Optimization. In *Advances in Neural Information Processing Systems (NeurIPS)*, 2024.
- [HG⁺19] N. Houlsby, A. Giurghi, et al. Parameter-efficient transfer learning for NLP. In *International Conference on Machine Learning (ICML)*, 2019.
- [HMT11] N. Halko, P.-G. Martinsson, and J. A. Tropp. Finding structure with randomness: Probabilistic algorithms for constructing approximate matrix decompositions. *SIAM Review*, 53(2):217–288, 2011.
- [HMZ⁺23] M. Huh, H. Mobahi, R. Zhang, B. Cheung, P. Agrawal, and P. Isola. The Low-Rank Simplicity Bias in Deep Networks. *Transactions on Machine Learning Research*, 2023.
- [HS⁺19] E. J. Hu, Y. Shen, et al. Lora: Low-rank adaptation of large language models. In *International Conference on Learning Representations (ICLR)*, 2019.
- [HUSN84] J.-B. Hiriart-Urruty, J.-J. Strodiot, and V. H. Nguyen. Generalized Hessian matrix and second-order optimality conditions for problems with $C^{1,1}$ data. *Appl. Math. Optim.*, 11(1):43–56, 1984.
- [KB15] D. P. Kingma and J. Ba. Adam: A Method for Stochastic Optimization. In *International Conference on Learning Representations (ICLR)*, 2015.
- [KBV09] Y. Koren, R. Bell, and C. Volinsky. Matrix Factorization Techniques for Recommender Systems. *Computer*, 42(8):30–37, 2009.
- [KJ⁺25] O. Khade, S. Jagdale, et al. Challenges in Adapting Multilingual LLMs to Low-Resource Languages using LoRA PEFT Tuning. In *Proceedings of the First Workshop on Challenges in Processing South Asian Languages (CHiPSAL 2025)*, Abu Dhabi, UAE, 2025. International Committee on Computational Linguistics.
- [KM23] C. Kümmerle and J. Maly. Recovering simultaneously structured data via non-convex iteratively reweighted least squares. In *Advances in Neural Information Processing Systems (NeurIPS)*, 2023.
- [KMV21] C. Kümmerle and C. Mayrink Verdun. A scalable second order method for ill-conditioned matrix completion from few samples. In *International Conference on Machine Learning (ICML)*, 2021.
- [Kor09] Y. Koren. The BellKor Solution to the Netflix Grand Prize. *Netflix prize documentation*, 81(2009):1–10, 2009.
- [Kri09] A. Krizhevsky. Learning Multiple Layers of Features from Tiny Images. *BibSonomy*, pages 32–33, 2009.
- [KS18] C. Kümmerle and J. Sigl. Harmonic Mean Iteratively Reweighted Least Squares for Low-Rank Matrix Recovery. *J. Mach. Learn. Res.*, 19(47):1–49, 2018.
- [KTMF21] S. Kamalakara, N. Tenenholtz, L. Mackey, and N. Fusi. Initialization and Regularization of Factorized Neural Layers. In *International Conference on Learning Representations (ICLR 2021)*, 2021.

- [Lew95] A. S. Lewis. The Convex Analysis of Unitarily Invariant Matrix Functions. *J. Convex Anal.*, 2(1–2):173–183, 1995.
- [LFX⁺24] A. Liu, B. Feng, B. Xue, B. Wang, B. Wu, C. Lu, C. Zhao, C. Deng, C. Zhang, C. Ruan, et al. DeepSeek-V3 Technical Report. *CoRR*, abs/2412.19437, 2024.
- [LH19] I. Loshchilov and F. Hutter. Decoupled Weight Decay Regularization. In *International Conference on Learning Representations (ICLR)*, 2019.
- [LHLZ24] Y. Luo, W. Huang, X. Li, and A. Zhang. Recursive importance sketching for rank constrained least squares: Algorithms and high-order convergence. *Operations Research*, 72(1):237–256, 2024.
- [LS05] A. S. Lewis and H. S. Sendov. Nonsmooth Analysis of Singular Values. Part I: Theory. *Set-Valued Analysis*, 13(3):213–241, 2005.
- [LS⁺23] V. Lialin, N. Shivagunde, et al. ReLoRA: High-Rank Training Through Low-Rank Updates. In *Workshop on Advancing Neural Network Training at Advances in Neural Information Processing Systems (WANT@NeurIPS)*, 2023.
- [LW⁺24] S.-Y. Liu, C.-Y. Wang, et al. Dora: Weight-decomposed low-rank adaptation. In *International Conference on Machine Learning*, 2024.
- [MF10] K. Mohan and M. Fazel. Reweighted nuclear norm minimization with application to system identification. In *Proceedings of the American Control Conference*, pages 2953–2959. IEEE, 2010.
- [MHP25] Z. Mo, L.-K. Huang, and S. J. Pan. Parameter and memory efficient pretraining via low-rank riemannian optimization. In *International Conference on Learning Representations (ICLR 2025)*, 2025.
- [MHR21] R. K. Mahabadi, J. Henderson, and S. Ruder. COMPACTER: efficient low-rank hypercomplex adapter layers. In *Advances in Neural Information Processing Systems (NeurIPS)*, 2021.
- [MNA⁺18] P. Micikevicius, S. Narang, J. Alben, G. Diamos, E. Elsen, D. Garcia, B. Ginsburg, M. Houston, O. Kuchaiev, G. Venkatesh, and H. Wu. Mixed Precision Training. In *International Conference on Learning Representations (ICLR)*, 2018.
- [MWCC20] C. Ma, K. Wang, Y. Chi, and Y. Chen. Implicit Regularization in Nonconvex Statistical Estimation: Gradient Descent Converges Linearly for Phase Retrieval, Matrix Completion, and Blind Deconvolution. *Foundations of Computational Mathematics*, 20:451–632, 2020.
- [Nat95] B. Natarajan. Sparse Approximate Solutions to Linear Systems. *SIAM J. Comput.*, 24(2):227–234, 1995.
- [RBD25] A. Radhakrishnan, M. Belkin, and D. Drusvyatskiy. Linear Recursive Feature Machines provably recover low-rank matrices. *Proceedings of the National Academy of Sciences*, 122(13):e2411325122, 2025.
- [RFP10] B. Recht, M. Fazel, and P. A. Parrilo. Guaranteed Minimum-Rank Solutions of Linear Matrix Equations via Nuclear Norm Minimization. *SIAM Review*, 52(3):471–501, 2010.
- [RKZK22] S. Rendle, W. Krichene, L. Zhang, and Y. Koren. Revisiting the Performance of iALS on Item Recommendation Benchmarks. In *Proceedings of the 16th ACM Conference on Recommender Systems, RecSys ’22*, page 427–435. Association for Computing Machinery, 2022.
- [RWC⁺19] A. Radford, J. Wu, R. Child, D. Luan, D. Amodei, and I. Sutskever. Language Models are Unsupervised Multitask Learners. *OpenAI Blog*, 2019. Technical report.

- [SKZ⁺22] A. P. Steiner, A. Kolesnikov, X. Zhai, R. Wightman, J. Uszkoreit, and L. Beyer. How to train your ViT? Data, Augmentation, and Regularization in Vision Transformers. *Transactions on Machine Learning Research*, 2022.
- [SL16] R. Sun and Z. Q. Luo. Guaranteed Matrix Completion via Non-Convex Factorization. *IEEE Trans. Inf. Theory*, 62(11):6535–6579, 2016.
- [SZ⁺23] D. Savostianova, E. Zangrando, et al. Robust Low-Rank Training via Orthonormal Constraints. In *Advances in Neural Information Processing Systems (NeurIPS)*, 2023.
- [SZ25] D. Stöger and Y. Zhu. Non-convex matrix sensing: Breaking the quadratic rank barrier in the sample complexity. In *Proceedings of the 38th Annual Conference on Learning Theory*, Proceedings of Machine Learning Research, 2025.
- [WAUc⁺23] H. Wang, S. Agarwal, P. Uchupala, Y. Tanaka, E. Xing, and D. Papailiopoulos. Cuttlefish: Low-Rank Model Training without All the Tuning. In *Proceedings of Machine Learning and Systems (MLSys 2023)*, 2023.
- [Wei37] E. Weiszfeld. Sur le point pour lequel la somme des distances de n points donnés est minimum. *Tohoku Mathematical Journal, First Series*, 43:355–386, 1937.
- [WMP⁺24] X. Wei, S. Moalla, R. Pascanu, et al. Building on Efficient Foundations: Effective Training of LLMs with Structured Feedforward Layers. In *Advances in Neural Information Processing Systems (NeurIPS)*, 2024.
- [WMPG24] X. Wei, S. Moalla, R. Pascanu, and C. Gulcehre. Investigating Low-Rank Training in Transformer Language Models: Efficiency and Scaling Analysis. In *ICML 2024 Workshop on “Next Generation of Sequence Modeling Architectures”*, 2024.
- [WP09] E. Weiszfeld and F. Plastria. On the point for which the sum of the distances to n given points is minimum. *Ann. Oper. Res.*, 167(1):7–41, Mar 2009.
- [XL⁺20] Y. Xu, Y. Li, et al. TRP: Trained Rank Pruning for Efficient Deep Neural Networks. In *Proceedings of the Twenty-Ninth International Joint Conference on Artificial Intelligence, IJCAI-20*, 2020.
- [XS⁺23] X. Xu, Y. Shen, et al. The power of preconditioning in overparameterized low-rank matrix sensing. In *International Conference on Machine Learning (ICML)*, 2023.
- [YATC20] H. Yang, P. Antonante, V. Tzoumas, and L. Carlone. Graduated Non-Convexity for Robust Spatial Perception: From Non-Minimal Solvers to Global Outlier Rejection. *IEEE Robotics and Automation Letters*, 5(2):1127–1134, 2020.
- [YCS⁺20] F. Yang, X. Chen, W. Shao, S.-F. Chang, and W. Liu. Learning Low-Rank Deep Neural Networks via Singular Vector Decomposition. In *IEEE/CVF Conference on Computer Vision and Pattern Recognition Workshops (CVPRW)*, pages 954–963, 2020.
- [YT⁺20] H. Yang, M. Tang, et al. Learning Low-Rank Deep Neural Networks via Singular Vector Orthogonality Regularization and Singular Value Sparsification. In *Proceedings of the IEEE/CVF Conference on Computer Vision and Pattern Recognition (CVPR) Workshops*, 2020.
- [YYT⁺20] F. Yan, Y. Yang, Y. Tang, et al. Learning Low-Rank Deep Neural Networks via Singular Vector Decomposition. In *Proceedings of the IEEE/CVF Conference on Computer Vision and Pattern Recognition Workshops (CVPRW)*, 2020.
- [ZCZ22] J. Zhang, H.-M. Chiu, and R. Y. Zhang. Accelerating SGD for Highly Ill-Conditioned Huge-Scale Online Matrix Completion. In *Advances in Neural Information Processing Systems (NeurIPS)*, 2022.
- [ZHSJ20] J. Zhang, T. He, S. Sra, and A. Jadbabaie. Why gradient clipping accelerates training: A theoretical justification for adaptivity, 2020.

- [ZL15] Q. Zheng and J. Lafferty. A Convergent Gradient Descent Algorithm for Rank Minimization and Semidefinite Programming from Random Linear Measurements. In *Advances in Neural Information Processing Systems (NeurIPS)*, 2015.
- [ZN22] P. Zilber and B. Nadler. GNMR: a provable one-line algorithm for low rank matrix recovery. *SIAM J. Math. Data Sci.*, 4(2):909–934, 2022.
- [ZZC⁺24] J. Zhao, Z. Zhang, B. Chen, Z. Wang, A. Anandkumar, and Y. Tian. GaLore: Memory-Efficient LLM Training by Gradient Low-Rank Projection. *ICML*, 2024.

Supplementary material for Q3R: *Quadratic Reweighted Rank Regularizer for Effective Low-Rank Training*

In this supplementary material, we first provide theoretical justifications of the relationship between Q3R and the smoothed objective, expanding on Section 4.1, in Section A. The derivation of a Q3R value evaluation algorithm is provided in Section B. The expression used in AdamQ3R is derived in Section C. In Section D, we discuss more experimental results in both pre-training and fine-tuning, and we discuss the computational aspects. In the concluding part of this supplementary material, in Section E, we demonstrate the robustness of Q3R to hyperparameter variation.

A Relationship between Smoothed Log-Determinant and Q3R

In this section, we expand on the relationship between the ϵ -smoothed log-determinant surrogate objective $F_\epsilon(\cdot)$ defined in (1). Part of this material is covered in [KM23, Section B.2] in a different context.

A.1 Properties of Smoothed Log-Determinant

We focus first on some basic properties of the ϵ -smoothed log-determinant $F_\epsilon : \mathbb{R}^{d_1 \times d_2} \rightarrow \mathbb{R}$, which, as we recall from (1), was defined for any $\mathbf{W} \in \mathbb{R}^{d_1 \times d_2}$ as

$$F_\epsilon(\mathbf{W}) := \sum_{i=1}^d f_\epsilon(\sigma_i(\mathbf{W})), \text{ where } f_\epsilon(\sigma) = \begin{cases} \epsilon^2 (\log(\sigma) - \log(\epsilon)) + \frac{1}{2}\epsilon^2, & \text{if } \sigma \geq \epsilon, \\ \frac{1}{2}\sigma^2, & \text{if } \sigma < \epsilon, \end{cases}$$

given $\epsilon > 0$.

As seen by its definition, $F_\epsilon(\cdot)$ is a *spectral function*, i.e., it only depends on the singular values $\sigma_1(\mathbf{W}), \sigma_2(\mathbf{W}), \dots$ of \mathbf{W} , but not on any singular vector information.

Let now $d := \min(d_1, d_2)$. More precisely, we can define, following [Lew95, Bec17, LS05], a *spectral function* $F : \mathbb{R}^{d_1 \times d_2} \rightarrow \mathbb{R}$ as a function for which there exists a function $f : \mathbb{R}^d \rightarrow \mathbb{R}$ for which $F = f \circ \sigma$, where $\sigma : \mathbb{R}^{d_1 \times d_2} \rightarrow \mathbb{R}^d$, $\mathbf{W} \mapsto \sigma(\mathbf{W}) = (\sigma_1(\mathbf{W}), \dots, \sigma_d(\mathbf{W}))$ is the function mapping matrices in $\mathbb{R}^{d_1 \times d_2}$ to its singular value vector $\sigma(\mathbf{W})$. A key towards understanding the derivative structure is that we can obtain an explicit formula for the gradient $\nabla F(\mathbf{W})$ of F_ϵ at \mathbf{W} if the function f in the spectral function definition is absolutely (permutation) symmetric [Bec17, Section 7.3] according to Definition A.1. It is easy to check that f_ϵ from the definition of the ϵ -smoothed log-determinant $F_\epsilon(\cdot)$ satisfies this definition.

Definition A.1 (Absolutely permutation symmetric functions). *1. Let $\mathbf{x} \in \mathbb{R}^d$. We call $r(\mathbf{x}) \in \mathbb{R}^d$ the non-increasing rearrangement of \mathbf{x} if it holds that*

$$r(\mathbf{x})_1 \geq r(\mathbf{x})_2 \geq \dots \geq r(\mathbf{x})_d$$

and there is a permutation matrix $\mathbf{P} \in \mathbb{P}^d$ such that $r(\mathbf{x})_i = (\mathbf{P}\mathbf{x})_i$ for all $i \in [d]$.

2. We say that a function $f : \mathbb{R}^d \rightarrow \mathbb{R}$ is absolutely permutation symmetric if

$$f(\mathbf{x}) = f(r(|\mathbf{x}|)) \tag{9}$$

for any $\mathbf{x} \in \mathbb{R}^d$.

For ease of notation, given a vector $\mathbf{v} \in \mathbb{R}^d$, we define $\text{dg}(\mathbf{v}) \in \mathbb{R}^{d_1 \times d_2}$ to be the rectangular diagonal matrix such that for $v \in \mathbb{R}^d$ and any $i \in \{1, \dots, d_1\}, j \in \{1, \dots, d_2\}$,

$$\text{dg}(\mathbf{v})_{ij} = \begin{cases} v_i, & \text{if } i = j, \\ 0, & \text{else.} \end{cases}$$

Next, we cite a key result about the differentiability of spectral functions, which is due to [LS05, Section 7].

Proposition A.1 (Differentiability of Spectral Functions [LS05, Section 7]). *Let $F : \mathbb{R}^{d_1 \times d_2} \rightarrow \mathbb{R}$ be a spectral function $F = f \circ \sigma$ with an associated function $f : \mathbb{R}^d \rightarrow \mathbb{R}$ that is absolutely permutation symmetric. Then, F is differentiable at $\mathbf{W} \in \mathbb{R}^{d_1 \times d_2}$ if and only if f is differentiable at $\sigma(\mathbf{W}) \in \mathbb{R}^d$.*

In this case, the gradient ∇F of F at \mathbf{W} is given by

$$\nabla F(\mathbf{W}) = \mathbf{U} \operatorname{dg}(\nabla f(\sigma(\mathbf{W}))) \mathbf{V}^\top$$

if $\mathbf{W} = \mathbf{U} \operatorname{dg}(\sigma(\mathbf{W})) \mathbf{V}^\top$ is a singular value decomposition of \mathbf{W} with orthogonal matrices $\mathbf{U} \in \mathbb{R}^{d_1 \times d_1}$ and $\mathbf{V} \in \mathbb{R}^{d_2 \times d_2}$.

Using Theorem A.1, we can characterize the derivative of the F_ϵ for arbitrary $\epsilon > 0$, as established in the following lemma.

Lemma A.2. *Let $\epsilon > 0$ and $F_\epsilon : \mathbb{R}^{d_1 \times d_2} \rightarrow \mathbb{R}$ be the ϵ -smoothed log-determinant of Equation (1). Then F_ϵ is differentiable with 1-Lipschitz gradient $\nabla F_\epsilon : \mathbb{R}^{d_1 \times d_2} \rightarrow \mathbb{R}^{d_1 \times d_2}$ that is given by*

$$\nabla F_\epsilon(\mathbf{W}) = \mathbf{U}_\mathbf{W} \operatorname{dg} \left(\frac{\sigma_i(\mathbf{W})}{\max(\sigma_i(\mathbf{W})/\epsilon, 1)^2} \right)_{i=1}^d \mathbf{V}_\mathbf{W}^\top \quad (10)$$

for any matrix \mathbf{W} with singular value decomposition $\mathbf{W} = \mathbf{U}_\mathbf{W} \operatorname{dg}(\sigma(\mathbf{W})) \mathbf{V}_\mathbf{W}^\top = \mathbf{U}_\mathbf{W} \operatorname{dg}(\sigma) \mathbf{V}_\mathbf{W}^\top$.

Proof of Theorem A.2. For the differentiability of F_ϵ , as per Theorem A.1, it is sufficient to show that the function $f((\sigma_1, \dots, \sigma_d)) = \sum_{i=1}^d f_\epsilon(\sigma_i)$ with $f_\epsilon : \mathbb{R}_{\geq 0} \rightarrow \mathbb{R}$ as defined in (1) is differentiable at any $(\sigma_1, \dots, \sigma_d) \in \mathbb{R}_{\geq 0}^d$. Due to the sum structure of f , this will follow if f_ϵ is itself differentiable at any $\sigma \geq 0$.

To this, we observe that for any $\sigma > 0, \sigma \neq \epsilon$, we have that f_ϵ is differentiable at σ with derivative

$$f'_\epsilon(\sigma) = \begin{cases} \frac{\epsilon^2}{\sigma}, & \text{if } \sigma > \epsilon \\ \sigma, & \text{if } 0 \leq \sigma < \epsilon. \end{cases}$$

Since $\lim_{\sigma \nearrow \epsilon} f'_\epsilon(\sigma) = \epsilon = \lim_{\sigma \searrow \epsilon} f'_\epsilon(\sigma)$, it follows that f_ϵ is also differentiable at $\sigma = \epsilon$ with $f'_\epsilon(\epsilon) = \epsilon$, and thus, differentiable on the entirety of its domain. The formula (10) follows then directly from Theorem A.1. \square

Remark A.3. It is well-known that the optimization of *convex* functions [BV04] is from many perspectives less challenging than the optimization of non-convex functions. In Section 4.1, we have claimed that the ϵ -smoothed log-determinant surrogate is *not* convex. This can indeed be shown directly by invoking [LS05, Proposition 6.1], which states that a spectral function $F = f \circ \sigma$ is convex if and only if f is convex. Indeed, it is easy to see that $f_\epsilon(\cdot)$ is not convex due to its logarithmic dependence on the input for large inputs, which shows that $F_\epsilon(\cdot)$ is not a convex function.

As mentioned in Section 4.1, we see from (10) that computing $\nabla F_\epsilon(\mathbf{W})$ given the matrix $\mathbf{W} \in \mathbb{R}^{d_1 \times d_2}$ indeed would require a *full* singular value decomposition that includes at least d leading singular values. Defining $r(\mathbf{W}, \epsilon) := |\{i \in \{1, \dots, d\} : \sigma_i(\mathbf{W}) > \epsilon\}|$ as in (3) and $\Sigma = \operatorname{diag}(\sigma_i(\mathbf{W}))_{i=1}^{r(\mathbf{W}, \epsilon)} \in \mathbb{R}^{r(\mathbf{W}, \epsilon) \times r(\mathbf{W}, \epsilon)}$ as in (4), we obtain for \mathbf{U} and \mathbf{V} defined from the $r(\mathbf{W}, \epsilon)$ leading columns of $\mathbf{U}_\mathbf{W} = [\mathbf{U} \quad \mathbf{U}_\perp] \in \mathbb{R}^{d_1 \times d_1}$ and $\mathbf{V}_\mathbf{W} = [\mathbf{V} \quad \mathbf{V}_\perp] \in \mathbb{R}^{d_2 \times d_2}$ that

$$\nabla F_\epsilon(\mathbf{W}) = \epsilon^2 \mathbf{U} \Sigma^{-1} \mathbf{V}^\top + \mathbf{U}_\perp \Sigma_\perp \mathbf{V}_\perp^\top, \quad (11)$$

inserting the formula from (10), with the notation that $\Sigma_\perp = \operatorname{dg}(\sigma_i(\mathbf{W}))_{i=r(\mathbf{W}, \epsilon)+1}^d$. Fundamentally, this is the key reason why a direct inclusion of the smoothed log-determinant objective into a gradient-based optimization algorithm is computationally inefficient.

Finally, we conclude with the observation that $F_\epsilon(\cdot)$ becomes *convex* if $\epsilon \gg 0$ is chosen large enough. In particular, it holds for any $\mathbf{W} \in \mathbb{R}^{d_1 \times d_2}$ that

$$F_\epsilon(\mathbf{W}) = \sum_{i=1}^d f_\epsilon(\sigma_i(\mathbf{W})) = \sum_{i=1}^d \frac{1}{2} \sigma_i^2(\mathbf{W}) = \frac{1}{2} \|\mathbf{W}\|_F^2$$

if additionally the largest singular value $\sigma_1(\mathbf{W})$ of \mathbf{W} satisfies $\sigma_1(\mathbf{W}) \leq \epsilon$. Here, we used in the last equality that the Frobenius norm of a matrix is the ℓ_2 -norm if its singular values.

A.2 The Quadratic Model Function Underlying Q3R

We proceed by justifying the claims made in Section 4.1 about the relationship between the ϵ -smoothed log-determinant $F_\epsilon(\cdot)$, the Q3R-regularizer $\text{Q3R}_{\mathbf{W}',\epsilon}(\cdot)$, the quadratic model $Q_\epsilon(\cdot \mid \mathbf{W}')$ of (2) and the reweighting operator $\mathcal{R}_{\mathbf{W}',\epsilon}(\cdot)$. To this end, we show the first statements of Theorem A.2 that characterize the reweighting operator $\mathcal{R}_{\mathbf{W}',\epsilon}(\cdot)$.

Proof of Theorem 4.1.1. Let $\mathbf{W}' \in \mathbb{R}^{d_1 \times d_2}$ be arbitrary with singular value decomposition $\mathbf{W}' = \mathbf{U}' \text{dg}(\sigma_i(\mathbf{W}')) \mathbf{V}'^\top$. Recall from Definition 4.1 that

$$\mathcal{R}_{\mathbf{W}',\epsilon}(\mathbf{W}) = \mathbf{U}' \Sigma_{\epsilon,d_1}^{-1} \mathbf{U}'^\top \mathbf{W} \mathbf{V}' \Sigma_{\epsilon,d_2}^{-1} \mathbf{V}'^\top,$$

where $\Sigma_{\epsilon,d} = \text{diag}(\max(\sigma_i(\mathbf{W}')/\epsilon, 1))_{i=1}^d \in \mathbb{R}^{d \times d}$ for $d \in \{d_1, d_2\}$.

To show that $\mathcal{R}_{\mathbf{W}',\epsilon} : \mathbb{R}^{d_1 \times d_2} \rightarrow \mathbb{R}^{d_1 \times d_2}$ is a positive definite operator, we consider any $\mathbf{W} \in \mathbb{R}^{d_1 \times d_2}$ such that $\mathbf{W} \neq 0$, which implies that $\|\mathbf{W}\|_F > 0$. Defining $\mathbf{Z} := \mathbf{U}'^\top \mathbf{W} \mathbf{V}'$, we see that

$$\begin{aligned} \langle \mathbf{W}, \mathcal{R}_{\mathbf{W}',\epsilon}(\mathbf{W}) \rangle &= \text{tr}(\mathbf{W}^\top \mathcal{R}_{\mathbf{W}',\epsilon}(\mathbf{W})) = \text{tr}(\mathbf{W}^\top \mathbf{U}' \Sigma_{\epsilon,d_1}^{-1} \mathbf{U}'^\top \mathbf{W} \mathbf{V}' \Sigma_{\epsilon,d_2}^{-1} \mathbf{V}'^\top) \\ &= \text{tr}(\mathbf{V}'^\top \mathbf{W}^\top \mathbf{U}' \Sigma_{\epsilon,d_1}^{-1} \mathbf{U}'^\top \mathbf{W} \mathbf{V}' \Sigma_{\epsilon,d_2}^{-1}) = \text{tr}(\mathbf{Z}^\top \Sigma_{\epsilon,d_1}^{-1} \mathbf{Z} \Sigma_{\epsilon,d_2}^{-1}) \\ &= \text{tr}((\Sigma_{\epsilon,d_1}^{-1} \mathbf{Z})^\top \mathbf{Z} \Sigma_{\epsilon,d_2}^{-1}) = \sum_{i=1}^{d_1} \sum_{j=1}^{d_2} (\Sigma_{\epsilon,d_1}^{-1} \mathbf{Z})_{ij} (\mathbf{Z} \Sigma_{\epsilon,d_2}^{-1})_{ij} \\ &= \sum_{i=1}^{d_1} \sum_{j=1}^{d_2} \tilde{\sigma}_i \tilde{\sigma}_j \mathbf{Z}_{ij}^2 \end{aligned}$$

with $\tilde{\sigma}_i := \max(\sigma_i(\mathbf{W}')/\epsilon, 1)^{-1}$ for $i \in \{1, \dots, \max(d_1, d_2)\}$, using the cyclicity of the trace in the third equality. Since $\tilde{\sigma}_i, \tilde{\sigma}_j > 0$ for all i, j (with convention that $\sigma_i(\mathbf{W}') = 0$ for $i > \min(d_1, d_2)$), we can establish the lower bound

$$\begin{aligned} \langle \mathbf{W}, \mathcal{R}_{\mathbf{W}',\epsilon}(\mathbf{W}) \rangle &= \sum_{i=1}^{d_1} \sum_{j=1}^{d_2} \tilde{\sigma}_i \tilde{\sigma}_j \mathbf{Z}_{ij}^2 \geq \min_{i=1}^{\max(d_1, d_2)} \tilde{\sigma}_i^2 \sum_{i=1}^{d_1} \sum_{j=1}^{d_2} \mathbf{Z}_{ij}^2 = \min_{i=1}^{\max(d_1, d_2)} \tilde{\sigma}_i^2 \|\mathbf{Z}\|_F^2 \\ &= \min_{i=1}^{\max(d_1, d_2)} \tilde{\sigma}_i^2 \|\mathbf{U}'^\top \mathbf{W} \mathbf{V}'\|_F^2 = \min_{i=1}^{\max(d_1, d_2)} \tilde{\sigma}_i^2 \|\mathbf{W}\|_F^2 > 0. \end{aligned}$$

□

Due to the definition of Q3R (6), an implication of this is that

$$\text{Q3R}_{\mathbf{W}',\epsilon}(\mathbf{W}) = \frac{1}{2} \langle \mathbf{W}, \mathcal{R}_{\mathbf{W}',\epsilon}(\mathbf{W}) \rangle \geq 0$$

and $\text{Q3R}_{\mathbf{W}',\epsilon}(\mathbf{W}) = 0 \Leftrightarrow \mathbf{W} = 0$, i.e., the value of Q3R is always non-negative and positive for non-zero matrices.

We proceed with the proof of the second statement of Theorem 4.1, which provides an explicit formula for the reweighting operator that only requires a partial SVD of \mathbf{W}' .

Proof of Theorem 4.1.2. If $\mathbf{W}' = \mathbf{U}_{\mathbf{W}'} \text{dg}(\sigma_i(\mathbf{W}')) \mathbf{V}_{\mathbf{W}'}^\top$ is a full singular value decomposition of \mathbf{W}' with $\mathbf{U}_{\mathbf{W}'} = [\mathbf{U} \quad \mathbf{U}_\perp] \in \mathbb{R}^{d_1 \times d_1}$ and $\mathbf{V}_{\mathbf{W}'} = [\mathbf{V} \quad \mathbf{V}_\perp] \in \mathbb{R}^{d_2 \times d_2}$, we recall that the image of a matrix $\mathbf{W} \in \mathbb{R}^{d_1 \times d_2}$ with respect to $\mathcal{R}_{\mathbf{W}',\epsilon}$ is defined (see Definition 4.1) as

$$\mathcal{R}_{\mathbf{W}',\epsilon}(\mathbf{W}) = \mathbf{U}_{\mathbf{W}'} \Sigma_{\epsilon,d_1}^{-1} \mathbf{U}_{\mathbf{W}'}^\top \mathbf{W} \mathbf{V}_{\mathbf{W}'} \Sigma_{\epsilon,d_2}^{-1} \mathbf{V}_{\mathbf{W}'}^\top, \quad (12)$$

using the definition for $\Sigma_{\epsilon,d}$ from the proof of Theorem 4.1.1 above.

With a similar argument as made in (11), we can see that

$$\mathbf{U}_{\mathbf{W}'} \Sigma_{\epsilon,d_1}^{-1} \mathbf{U}_{\mathbf{W}'}^\top = \epsilon \mathbf{U} \Sigma^{-1} \mathbf{U}^\top + \mathbf{U}_\perp \mathbf{U}_\perp^\top = \epsilon \mathbf{U} \Sigma^{-1} \mathbf{U}^\top + \mathbf{I} - \mathbf{U} \mathbf{U}^\top$$

with $\Sigma = \text{diag}(\sigma_i(\mathbf{W}'))_{i=1}^{r(\mathbf{W}', \epsilon)} \in \mathbb{R}^{r(\mathbf{W}', \epsilon) \times r(\mathbf{W}', \epsilon)}$, $\mathbf{U} \in \mathbb{R}^{d_1 \times r(\mathbf{W}', \epsilon)}$ and the identity matrix \mathbf{I} . In the last equation, we used that $\mathbf{U}_\perp \mathbf{U}_\perp^\top$ is the projection operator onto the subspace that is *orthogonal* to the one spanned by the columns of \mathbf{U} . Analogously, we obtain that

$$\mathbf{V}_{\mathbf{W}', \epsilon} \Sigma_{\epsilon, d_2}^{-1} \mathbf{V}_{\mathbf{W}'}^\top = \epsilon \mathbf{V} \Sigma^{-1} \mathbf{V}^\top + \mathbf{V}_\perp \mathbf{V}_\perp^\top = \epsilon \mathbf{V} \Sigma^{-1} \mathbf{V}^\top + \mathbf{I} - \mathbf{V} \mathbf{V}^\top,$$

where $\mathbf{V} \in \mathbb{R}^{d_2 \times r(\mathbf{W}', \epsilon)}$. Inserting these two equations into (12), we obtain

$$\begin{aligned} \mathcal{R}_{\mathbf{W}', \epsilon}(\mathbf{W}) &= \mathbf{U}_{\mathbf{W}'} \Sigma_{\epsilon, d_1}^{-1} \mathbf{U}_{\mathbf{W}'}^\top \mathbf{W} \mathbf{V}_{\mathbf{W}', \epsilon} \Sigma_{\epsilon, d_2}^{-1} \mathbf{V}_{\mathbf{W}'}^\top = \\ &= (\epsilon \mathbf{U} \Sigma^{-1} \mathbf{U}^\top + \mathbf{I} - \mathbf{U} \mathbf{U}^\top) \mathbf{W} (\epsilon \mathbf{V} \Sigma^{-1} \mathbf{V}^\top + \mathbf{I} - \mathbf{V} \mathbf{V}^\top) \\ &= \epsilon^2 \mathbf{U} \Sigma^{-1} \mathbf{U}^\top \mathbf{W} \mathbf{V} \Sigma^{-1} \mathbf{V}^\top + \epsilon \mathbf{U} \Sigma^{-1} \mathbf{U}^\top \mathbf{W} (\mathbf{I} - \mathbf{V} \mathbf{V}^\top) \\ &\quad + \epsilon (\mathbf{I} - \mathbf{U} \mathbf{U}^\top) \mathbf{W} \mathbf{V} \Sigma^{-1} \mathbf{V}^\top + (\mathbf{I} - \mathbf{U} \mathbf{U}^\top) \mathbf{W} (\mathbf{I} - \mathbf{V} \mathbf{V}^\top), \end{aligned}$$

where the last equality shows the statement of Theorem 4.1.2. \square

As a preparation for the proof of the last statement of Theorem 4.1, we formulate the following lemma which relates the gradient of F_ϵ at \mathbf{W} with the reweighting operator.

Lemma A.4 (Gradient Condition). *Let $\epsilon > 0$. For any $\mathbf{W} \in \mathbb{R}^{d_1 \times d_2}$, the reweighting operator $\mathcal{R}_{\mathbf{W}, \epsilon} : \mathbb{R}^{d_1 \times d_2} \rightarrow \mathbb{R}^{d_1 \times d_2}$ satisfies*

$$\mathcal{R}_{\mathbf{W}, \epsilon}(\mathbf{W}) = \nabla F_\epsilon(\mathbf{W}), \quad (13)$$

where $\nabla F_\epsilon(\mathbf{W})$ is the gradient of the ϵ -smoothed log-determinant at \mathbf{W} .

Proof. If $\mathbf{W} = \mathbf{U}_{\mathbf{W}} \text{dg}(\sigma_i(\mathbf{W})) \mathbf{V}_{\mathbf{W}}^\top$ is a singular value decomposition of \mathbf{W} with $\mathbf{U}_{\mathbf{W}} = [\mathbf{U} \quad \mathbf{U}_\perp] \in \mathbb{R}^{d_1 \times d_1}$ and $\mathbf{V}_{\mathbf{W}} = [\mathbf{V} \quad \mathbf{V}_\perp] \in \mathbb{R}^{d_2 \times d_2}$, we observe that

$$\begin{aligned} \mathcal{R}_{\mathbf{W}, \epsilon}(\mathbf{W}) &= \mathbf{U}_{\mathbf{W}} \Sigma_{\epsilon, d_1}^{-1} \mathbf{U}_{\mathbf{W}}^\top (\mathbf{U}_{\mathbf{W}} \text{dg}(\sigma_i(\mathbf{W})) \mathbf{V}_{\mathbf{W}}^\top) \mathbf{V}_{\mathbf{W}} \Sigma_{\epsilon, d_2}^{-1} \mathbf{V}_{\mathbf{W}}^\top \\ &= \mathbf{U}_{\mathbf{W}} \Sigma_{\epsilon, d_1}^{-1} \text{dg}(\sigma_i(\mathbf{W})) \Sigma_{\epsilon, d_2}^{-1} \mathbf{V}_{\mathbf{W}}^\top \\ &= \mathbf{U}_{\mathbf{W}} \text{dg} \left(\frac{\sigma_i(\mathbf{W})}{\max(\sigma_i(\mathbf{W})/\epsilon, 1)^2} \right)_{i=1}^d \mathbf{V}_{\mathbf{W}}^\top = \nabla F_\epsilon(\mathbf{W}), \end{aligned}$$

using the gradient formula Theorem A.2 in the last equality. \square

As a corollary of Theorem A.4, we see that for $\mathbf{W}' = \mathbf{W}$, the gradient of the Q3R regularizer satisfies

$$\nabla \text{Q3R}_{\mathbf{W}, \epsilon}(\mathbf{W}) = \nabla F_\epsilon(\mathbf{W}).$$

This is a direct implication of Theorem A.4 since

$$\nabla_{\mathbf{W}} \text{Q3R}_{\mathbf{W}' = \mathbf{W}, \epsilon}(\mathbf{W}) = \nabla_{\mathbf{W}} \left(\frac{1}{2} \langle \mathbf{W}, \mathcal{R}_{\mathbf{W}' = \mathbf{W}, \epsilon}(\mathbf{W}) \rangle \right) = \mathcal{R}_{\mathbf{W}, \epsilon}(\mathbf{W})$$

using the self-adjointness (see, e.g., [KM23, Appendix B]) of $\mathcal{R}_{\mathbf{W}, \epsilon}$.

The gradient condition (13) enables us to equate the definition of the quadratic model function (2) $Q_\epsilon(\cdot \mid \mathbf{W}')$ (which is, up to a constant that depends on ϵ and \mathbf{W}' the same as the value of Q3R) with the standard quadratic model form of (5).

Proof of Theorem 4.1.3. Let $\mathbf{W}, \mathbf{W}' \in \mathbb{R}^{d_1 \times d_2}$ be arbitrary. To show the equation (5), we start with its right hand side. By inserting (13), we obtain

$$\begin{aligned} &F_\epsilon(\mathbf{W}') + \langle \nabla F_\epsilon(\mathbf{W}'), \mathbf{W} - \mathbf{W}' \rangle + \frac{1}{2} \langle \mathbf{W} - \mathbf{W}', \mathcal{R}_{\mathbf{W}', \epsilon}(\mathbf{W} - \mathbf{W}') \rangle \\ &= F_\epsilon(\mathbf{W}') + \langle \mathcal{R}_{\mathbf{W}', \epsilon}(\mathbf{W}'), \mathbf{W} - \mathbf{W}' \rangle + \frac{1}{2} \langle \mathbf{W}, \mathcal{R}_{\mathbf{W}', \epsilon}(\mathbf{W}) \rangle - \langle \mathcal{R}_{\mathbf{W}', \epsilon}(\mathbf{W}'), \mathbf{W} \rangle \\ &\quad + \frac{1}{2} \langle \mathbf{W}', \mathcal{R}_{\mathbf{W}', \epsilon}(\mathbf{W}') \rangle \\ &= F_\epsilon(\mathbf{W}') + \frac{1}{2} \langle \mathbf{W}, \mathcal{R}_{\mathbf{W}', \epsilon}(\mathbf{W}) \rangle - \frac{1}{2} \langle \mathbf{W}', \mathcal{R}_{\mathbf{W}', \epsilon}(\mathbf{W}') \rangle \\ &=: Q_\epsilon(\mathbf{W} \mid \mathbf{W}'), \end{aligned}$$

where we also use the self-adjointness of $\mathcal{R}_{\mathbf{W}',\epsilon}(\cdot)$ in the first equality. The last expression corresponds to the definition of the quadratic model $Q_\epsilon(\cdot \mid \mathbf{W}')$ of $F_\epsilon(\cdot)$ given the expansion point \mathbf{W}' . This concludes the proof. \square

From this proof, it becomes clear that the quadratic model $Q_\epsilon(\cdot \mid \mathbf{W}')$ is a pure quadratic model with vanishing linear term. This implies that, for example, $Q_\epsilon(-\mathbf{W} \mid \mathbf{W}') = Q_\epsilon(\mathbf{W} \mid \mathbf{W}')$ for all \mathbf{W} , which reflects the geometry of the smoothed log-determinant $F_\epsilon(\cdot)$ better than a mixed quadratic model function as it likewise satisfies $F_\epsilon(-\mathbf{W}) = F_\epsilon(\mathbf{W})$.

B Computation of Regularizer Value of Q3R

In this section, we provide with Algorithm 3 below an implementable algorithm for evaluating the Q3R regularizer $\text{Q3R}_{\mathbf{W}',\epsilon}(\mathbf{W})$ of a weight matrix \mathbf{W} given, as defined in (6), given the reweighting operator $\mathcal{R}_{\mathbf{W}',\epsilon}(\cdot)$ of Definition 4.1 defined for the matrix \mathbf{W}' with leading left and right singular vector matrices $\mathbf{U} \in \mathbb{R}^{d_1 \times r}$ and $\mathbf{V} \in \mathbb{R}^{d_2 \times r}$ and leading r singular vectors $\sigma \in \mathbb{R}^r$, where $r = r(\mathbf{W}', \epsilon)$ as in (3).

We note that strictly speaking, evaluating $\text{Q3R}_{\mathbf{W}',\epsilon}(\mathbf{W})$ is never necessary in a training scheme such as AdamQ3R; however, evaluating $\text{Q3R}_{\mathbf{W}',\epsilon}(\mathbf{W})$ might be insightful to keep track of the extent of the regularization.

First, we decompose, following its definition (4), the reweighting operator image such that

$$\mathcal{R}_{\mathbf{W}',\epsilon}(\mathbf{W}) = T_1^\epsilon + T_2^\epsilon + T_3^\epsilon + T_4^\epsilon$$

with

$$\begin{aligned} T_1^\epsilon &= \epsilon^2 \mathbf{U} \Sigma^{-1} \mathbf{U}^\top \mathbf{W} \mathbf{V} \Sigma^{-1} \mathbf{V}^\top, \\ T_2^\epsilon &= \epsilon \mathbf{U} \Sigma^{-1} \mathbf{U}^\top \mathbf{W} (\mathbf{I} - \mathbf{V} \mathbf{V}^\top), \\ T_3^\epsilon &= \epsilon (\mathbf{I} - \mathbf{U} \mathbf{U}^\top) \mathbf{W} \mathbf{V} \Sigma^{-1} \mathbf{V}^\top, \\ T_4^\epsilon &= (\mathbf{I} - \mathbf{U} \mathbf{U}^\top) \mathbf{W} (\mathbf{I} - \mathbf{V} \mathbf{V}^\top). \end{aligned}$$

Defining

$$\begin{aligned} I_1 &= \langle \mathbf{W}, T_1^\epsilon \rangle = \epsilon^2 \text{tr}(\mathbf{W}^\top \mathbf{U} \Sigma^{-1} \mathbf{U}^\top \mathbf{W} \mathbf{V} \Sigma^{-1} \mathbf{V}^\top), \\ I_2 &= \langle \mathbf{W}, T_2^\epsilon \rangle = \epsilon \text{tr}(\mathbf{W}^\top \mathbf{U} \Sigma^{-1} \mathbf{U}^\top \mathbf{W} (\mathbf{I} - \mathbf{V} \mathbf{V}^\top)), \\ I_3 &= \langle \mathbf{W}, T_3^\epsilon \rangle = \epsilon \text{tr}(\mathbf{W}^\top (\mathbf{I} - \mathbf{U} \mathbf{U}^\top) \mathbf{W} \mathbf{V} \Sigma^{-1} \mathbf{V}^\top), \\ I_4 &= \langle \mathbf{W}, T_4^\epsilon \rangle = \text{tr}(\mathbf{W}^\top (\mathbf{I} - \mathbf{U} \mathbf{U}^\top) \mathbf{W} (\mathbf{I} - \mathbf{V} \mathbf{V}^\top)), \end{aligned}$$

and recalling the definition (6) of $\text{Q3R}_{\mathbf{W}',\epsilon}(\mathbf{W})$, we can write

$$\text{Q3R}_{\mathbf{W}',\epsilon}(\mathbf{W}) = \frac{1}{2} \langle \mathbf{W}, \mathcal{R}_{\mathbf{W}',\epsilon}(\mathbf{W}) \rangle = \frac{1}{2} (I_1 + I_2 + I_3 + I_4).$$

Below, we outline several steps that lead to an efficient implementation of the computation of the value of $\text{Q3R}_{\mathbf{W}',\epsilon}(\mathbf{W})$. **Apply cyclicity to I_1, I_2, I_3 .**

$$\begin{aligned} I_1 &= \epsilon^2 \text{tr}(\mathbf{V}^\top \mathbf{W}^\top \mathbf{U} \Sigma^{-1} \mathbf{U}^\top \mathbf{W} \mathbf{V} \Sigma^{-1}), \\ I_2 &= \epsilon \left[\text{tr}(\mathbf{W}^\top \mathbf{U} \Sigma^{-1} \mathbf{U}^\top \mathbf{W}) - \text{tr}(\mathbf{W}^\top \mathbf{U} \Sigma^{-1} \mathbf{U}^\top \mathbf{W} \mathbf{V} \mathbf{V}^\top) \right], \\ I_3 &= \epsilon \left[\text{tr}(\mathbf{W}^\top \mathbf{W} \mathbf{V} \Sigma^{-1} \mathbf{V}^\top) - \text{tr}(\mathbf{W}^\top \mathbf{U} \mathbf{U}^\top \mathbf{W} \mathbf{V} \Sigma^{-1} \mathbf{V}^\top) \right]. \end{aligned}$$

Expand I_4 .

$$I_4 = \text{tr}(\mathbf{W}^\top \mathbf{W}) - \text{tr}(\mathbf{W}^\top \mathbf{W} \mathbf{V} \mathbf{V}^\top) - \text{tr}(\mathbf{W}^\top \mathbf{U} \mathbf{U}^\top \mathbf{W}) + \text{tr}(\mathbf{W}^\top \mathbf{U} \mathbf{U}^\top \mathbf{W} \mathbf{V} \mathbf{V}^\top).$$

Group terms.

$$\begin{aligned}\langle \mathbf{W}, \mathcal{R}_{\mathbf{W}', \epsilon}(\mathbf{W}) \rangle &= \text{tr}(\mathbf{W}^\top \mathbf{W}) \\ &+ \epsilon^2 \text{tr}(\mathbf{V}^\top \mathbf{W}^\top \mathbf{U} \Sigma^{-1} \mathbf{U}^\top \mathbf{W} \mathbf{V} \Sigma^{-1}) \\ &+ \epsilon \text{tr}(\mathbf{W}^\top \mathbf{U} \Sigma^{-1} \mathbf{U}^\top \mathbf{W}) - \epsilon \text{tr}(\mathbf{W}^\top \mathbf{U} \Sigma^{-1} \mathbf{U}^\top \mathbf{W} \mathbf{V} \mathbf{V}^\top) \\ &+ \epsilon \text{tr}(\mathbf{W}^\top \mathbf{W} \mathbf{V} \Sigma^{-1} \mathbf{V}^\top) - \epsilon \text{tr}(\mathbf{W}^\top \mathbf{U} \mathbf{U}^\top \mathbf{W} \mathbf{V} \Sigma^{-1} \mathbf{V}^\top) \\ &- \text{tr}(\mathbf{W}^\top \mathbf{W} \mathbf{V} \mathbf{V}^\top) - \text{tr}(\mathbf{W}^\top \mathbf{U} \mathbf{U}^\top \mathbf{W}) + \text{tr}(\mathbf{W}^\top \mathbf{U} \mathbf{U}^\top \mathbf{W} \mathbf{V} \mathbf{V}^\top).\end{aligned}$$

Then by rearranging each pair of trace-terms we arrive at

$$\begin{aligned}\text{Q3R}_{\mathbf{W}', \epsilon}(\mathbf{W}) &= \frac{1}{2} \langle \mathbf{W}, \mathcal{R}_{\mathbf{W}', \epsilon}(\mathbf{W}) \rangle = \frac{1}{2} \left(\text{tr}(\mathbf{W}^\top \mathbf{W}) \right. \\ &\quad + \text{tr}(\mathbf{U}^\top \mathbf{W} \mathbf{W}^\top \mathbf{U} (\epsilon \Sigma^{-1} - \mathbf{I})) \\ &\quad + \text{tr}(\mathbf{V}^\top \mathbf{W}^\top \mathbf{W} \mathbf{V} (\epsilon \Sigma^{-1} - \mathbf{I})) \\ &\quad \left. + \text{tr}(\mathbf{V}^\top \mathbf{W}^\top \mathbf{U} (\epsilon \Sigma^{-1} - \mathbf{I}) \mathbf{U}^\top \mathbf{W} \mathbf{V} (\epsilon \Sigma^{-1} - \mathbf{I})) \right).\end{aligned}$$

For algorithmic simplicity, we now re-arrange the terms, leading to a simplified expression for this inner product in Algorithm 3: Rewriting these terms, we obtain

$$\begin{aligned}\text{Q3R}_{\mathbf{W}', \epsilon}(\mathbf{W}) &= \\ &= \frac{1}{2} \left(\underbrace{\text{tr}(\mathbf{W}^\top \mathbf{W})}_{t_1} + \underbrace{\text{tr}(\mathbf{V}^\top \mathbf{W}^\top \mathbf{U} \mathbf{S} \mathbf{U}^\top \mathbf{W} \mathbf{V} \mathbf{S})}_{t_2} + \underbrace{\text{tr}(\mathbf{V}^\top \mathbf{W}^\top \mathbf{W} \mathbf{V} \mathbf{S})}_{t_3} + \underbrace{\text{tr}(\mathbf{U}^\top \mathbf{W} \mathbf{W}^\top \mathbf{U} \mathbf{S})}_{t_4} \right),\end{aligned}$$

where $\mathbf{S} = \epsilon \Sigma^{-1} - \mathbf{I} = \text{diag}(\mathbf{s}_{\text{shift}})$, $\mathbf{A} = \mathbf{U}^\top \mathbf{W}$, $\mathbf{B} = \mathbf{W} \mathbf{V}$ and $\mathbf{C} = \mathbf{U}^\top \mathbf{W} \mathbf{V}$. Using $\text{tr}(\mathbf{A}^\top \mathbf{A}) = \|\mathbf{A}\|_F^2$ and cyclicity, we see that the t_i can be computed for $t = 1, 2, 3, 4$ such that

$$\begin{aligned}t_1 &= \|\mathbf{W}\|_F^2 = \sum_{i=1}^{d_1} \sum_{j=1}^{d_2} \mathbf{W}_{ij}^2, \\ t_2 &= \text{tr}(\mathbf{C}^\top \mathbf{S} \mathbf{C} \mathbf{S}) = \sum_{i=1}^r \sum_{j=1}^r (\mathbf{s}_{\text{shift}})_i (\mathbf{s}_{\text{shift}})_j \mathbf{C}_{ij}^2, \\ t_3 &= \text{tr}(\mathbf{B}^\top \mathbf{B} \mathbf{S}) = \sum_{i=1}^{d_1} \sum_{j=1}^r \mathbf{B}_{ij}^2 (\mathbf{s}_{\text{shift}})_j, \\ t_4 &= \text{tr}(\mathbf{A} \mathbf{A}^\top \mathbf{S}) = \sum_{i=1}^r \sum_{j=1}^{d_2} (\mathbf{s}_{\text{shift}})_i \mathbf{A}_{ij}^2.\end{aligned}$$

The outline of the resulting algorithm is as follows.

Algorithm 3 COMPUTATION OF Q3R FUNCTION VALUE $\text{Q3R}_{\mathbf{W}', \epsilon}(\mathbf{W})$

Input: $\mathbf{W} \in \mathbb{R}^{d_1 \times d_2}$, $\mathbf{U} \in \mathbb{R}^{d_1 \times r}$, $\mathbf{V} \in \mathbb{R}^{d_2 \times r}$, singular values $\sigma \in \mathbb{R}_{>0}^r$, smoothing parameter $\epsilon > 0$

Output: $\text{Q3R}_{\mathbf{W}', \epsilon}(\mathbf{W})$

- | | |
|--|---|
| 1: $\mathbf{s}_{\text{shift}} \leftarrow \epsilon / \max(\boldsymbol{\sigma}, \epsilon) - 1$
2: $\mathbf{A} \leftarrow \mathbf{U}^\top \mathbf{W}$
3: $\mathbf{B} \leftarrow \mathbf{W} \mathbf{V}$
4: $\mathbf{C} \leftarrow \mathbf{A} \mathbf{V}$
5: $t_1 \leftarrow \text{sum}(\text{sum}(\mathbf{W}^{\circ 2}, 1), 2)$
6: $t_2 \leftarrow \text{sum}(\text{sum}(\mathbf{s}_{\text{shift}} * \mathbf{C}^{\circ 2} * \mathbf{s}_{\text{shift}}, 1), 2)$
7: $t_3 \leftarrow \text{sum}(\text{sum}(\mathbf{B}^{\circ 2} * \mathbf{s}_{\text{shift}}, 1), 2)$
8: $t_4 \leftarrow \text{sum}(\text{sum}(\mathbf{s}_{\text{shift}} * \mathbf{A}^{\circ 2}, 1), 2)$
9: return $f \leftarrow (t_1 + t_2 + t_3 + t_4)/2$ | $\triangleright 2r$ multiplications and subtractions
$\triangleright (2r - 1)d_1 d_2$ additions and scalar products
$\triangleright (2r - 1)d_1 d_2$ additions and scalar products
$\triangleright (2r - 1)r d_2$ additions and scalar products
$\triangleright 2d_1 d_2 - 1$ additions and scalar products
$\triangleright 4r^2 - 1$ additions and scalar products
$\triangleright 3r d_1 - 1$ additions and scalar products
$\triangleright 3r d_2 - 1$ additions and scalar products
$\triangleright 3$ additions and 1 multiplication |
|--|---|
-

In Algorithm 3, we denote by $\mathbf{W}^{\circ 2}$ the matrix of entrywise squares of \mathbf{W} , by $\mathbf{s} * \mathbf{M}$ the row-wise scalar multiplication of \mathbf{s} with \mathbf{M} and by $\text{sum}(\cdot, 1)$ and $\text{sum}(\cdot, 2)$ row- and column-wise summation of matrix entries, respectively.

To summarize, we obtain a total FLOP count of

$$\text{FLOPs} = 4rd_1d_2 + 2r^2d_2 + 2rd_2 + 3rd_1 + 4r^2 + 2r = O(rd_1d_2)$$

for evaluating $\text{Q3R}_{\mathbf{W}', \epsilon}(\mathbf{W})$.

C Computation of the Gradient of Q3R

In this section, we outline a simple algorithm that, given reference weight matrix $\mathbf{W}' \in \mathbb{R}^{d_1 \times d_2}$, current layer weight matrix $\mathbf{W} \in \mathbb{R}^{d_1 \times d_2}$ and smoothing parameter $\epsilon > 0$, computes the gradient $\nabla_{\mathbf{W}} \text{Q3R}_{\mathbf{W}', \epsilon}(\mathbf{W})$ of the quadratic reweighted rank regularizer $\text{Q3R}_{\mathbf{W}', \epsilon}(\mathbf{W})$ defined in (6) of Section 4.1.

As mentioned in Section 4.2 and after the proof of Theorem 4.1.2, it follows from the self-adjointness of the reweighting operator $\mathcal{R}_{\mathbf{W}', \epsilon}(\cdot)$ that

$$\nabla_{\mathbf{W}} \text{Q3R}_{\mathbf{W}', \epsilon}(\mathbf{W}) = \nabla_{\mathbf{W}} \left(\frac{1}{2} \langle \mathbf{W}, \mathcal{R}_{\mathbf{W}', \epsilon}(\mathbf{W}) \rangle \right) = \mathcal{R}_{\mathbf{W}', \epsilon}(\mathbf{W})$$

From Equation (4), we rearrange the summand for algorithmic simplicity

$$\begin{aligned} \mathcal{R}_{\mathbf{W}', \epsilon}(\mathbf{W}) &= \epsilon^2 \mathbf{U} \mathbf{\Sigma}^{-1} \mathbf{U}^\top \mathbf{W} \mathbf{V} \mathbf{\Sigma}^{-1} \mathbf{V}^\top + \epsilon \mathbf{U} \mathbf{\Sigma}^{-1} \mathbf{U}^\top \mathbf{W} (\mathbf{I} - \mathbf{V} \mathbf{V}^\top) \\ &\quad + \epsilon (\mathbf{I} - \mathbf{U} \mathbf{U}^\top) \mathbf{W} \mathbf{V} \mathbf{\Sigma}^{-1} \mathbf{V}^\top + (\mathbf{I} - \mathbf{U} \mathbf{U}^\top) \mathbf{W} (\mathbf{I} - \mathbf{V} \mathbf{V}^\top). \end{aligned}$$

Using the equation $\epsilon \mathbf{\Sigma}^{-1} = \mathbf{I} + \mathbf{S}$ for the diagonal matrix $\mathbf{S} = \epsilon \mathbf{\Sigma}^{-1} - \mathbf{I}$, we can rewrite each term such that

$$\begin{aligned} T_1^\epsilon &:= \epsilon^2 \mathbf{U} \mathbf{\Sigma}^{-1} \mathbf{U}^\top \mathbf{W} \mathbf{V} \mathbf{\Sigma}^{-1} \mathbf{V}^\top = \mathbf{U} (\mathbf{I} + \mathbf{S}) \mathbf{U}^\top \mathbf{W} \mathbf{V} (\mathbf{I} + \mathbf{S}) \mathbf{V}^\top, \\ T_2^\epsilon &:= \epsilon \mathbf{U} \mathbf{\Sigma}^{-1} \mathbf{U}^\top \mathbf{W} (\mathbf{I} - \mathbf{V} \mathbf{V}^\top) = \mathbf{U} (\mathbf{I} + \mathbf{S}) \mathbf{U}^\top \mathbf{W} (\mathbf{I} - \mathbf{V} \mathbf{V}^\top), \\ T_3^\epsilon &:= \epsilon (\mathbf{I} - \mathbf{U} \mathbf{U}^\top) \mathbf{W} \mathbf{V} \mathbf{\Sigma}^{-1} \mathbf{V}^\top = (\mathbf{I} - \mathbf{U} \mathbf{U}^\top) \mathbf{W} \mathbf{V} (\mathbf{I} + \mathbf{S}) \mathbf{V}^\top, \\ T_4^\epsilon &:= (\mathbf{I} - \mathbf{U} \mathbf{U}^\top) \mathbf{W} (\mathbf{I} - \mathbf{V} \mathbf{V}^\top). \end{aligned}$$

Collecting like terms in powers of \mathbf{S} gives the compact form

$$\mathcal{R}_{\mathbf{W}', \epsilon}(\mathbf{W}) = \mathbf{W} + \underbrace{\mathbf{U} \mathbf{S} (\mathbf{U}^\top \mathbf{W} + \mathbf{U}^\top \mathbf{W} \mathbf{V} \mathbf{S} \mathbf{V}^\top)}_{T_2} + \underbrace{\mathbf{W} \mathbf{V} \mathbf{S} \mathbf{V}^\top}_{T_3}$$

with $\mathbf{S} = \epsilon \mathbf{\Sigma}^{-1} - \mathbf{I}$.

Now, we deduce the gradient in the following algorithm that is used in line 12 of Algorithm 2. We explain the step-by-step computation of our $\mathcal{R}_{\mathbf{W}', \epsilon}(\mathbf{W})$ stated below.

Algorithm 4 COMPUTATION OF Q3R GRADIENT : Compute $\nabla_{\mathbf{W}} \text{Q3R}_{\mathbf{W}', \epsilon}(\mathbf{W}) = \mathcal{R}_{\mathbf{W}', \epsilon}(\mathbf{W})$

Input: $\mathbf{W} \in \mathbb{R}^{d_1 \times d_2}$, $\mathbf{U} \in \mathbb{R}^{d_1 \times r}$, $\mathbf{V} \in \mathbb{R}^{d_2 \times r}$, singular values $\boldsymbol{\sigma} \in \mathbb{R}_{>0}^r$, smoothing parameter ϵ

Output: $\mathbf{G} = \mathcal{R}_{\mathbf{W}', \epsilon}(\mathbf{W})$

1: $\mathbf{s}_{\text{shift}} \leftarrow \epsilon / \max(\boldsymbol{\sigma}, \epsilon) - 1$	$\triangleright 2r$ multiplications and subtractions
2: $\mathbf{A} \leftarrow \mathbf{U}^\top \mathbf{W}$	$\triangleright (2r - 1)d_1d_2$ additions and scalar products
3: $\mathbf{B} \leftarrow \mathbf{W} \mathbf{V}$	$\triangleright (2r - 1)d_1d_2$ additions and scalar products
4: $\mathbf{C} \leftarrow \mathbf{A} \mathbf{V}$	$\triangleright (2r - 1)rd_2$ additions and scalar products
5: $\mathbf{E} \leftarrow \mathbf{U} * \mathbf{s}_{\text{shift}}$	$\triangleright d_1r$ scalar products
6: $\mathbf{F} \leftarrow \mathbf{V} * \mathbf{s}_{\text{shift}}$	$\triangleright d_2r$ scalar products
7: $\mathbf{T}_2 \leftarrow \mathbf{E}(\mathbf{A} + \mathbf{C} \mathbf{F}^\top)$	$\triangleright (2r - 1)(r + d_1)d_2$ additions and scalar products
8: $\mathbf{T}_3 \leftarrow \mathbf{B} \mathbf{F}^\top$	$\triangleright (2r - 1)d_1d_2$ additions and scalar products
9: $\text{grad} \leftarrow \mathbf{W} + \mathbf{T}_2 + \mathbf{T}_3$	$\triangleright 2d_1d_2$ elementwise additions
10: return grad	

The total number of floating point operations incurred by Algorithm 4 for computation of regularizer gradients $\nabla_{\mathbf{W}} \text{Q3R}_{\mathbf{W}, \epsilon}(\mathbf{W})$ is

$$\text{FLOPs} = 8rd_1d_2 - 2d_1d_2 + 4r^2d_2 + r(d_1 - d_2) + 2r = O(rd_1d_2).$$

D Experimental Results

In this section, we provide details regarding the experimental training methodology of Section 5 as well as some additional data of these experiments.

D.1 Experimental Protocol

In the experiments, we compared unregularized training with models regularized by Q3R, LoRITA [AZW24], and LoRA [HS⁺19]. Due to the limitations of some techniques in providing clear truncation guidelines, we truncate each method at a range of truncation ranks r . We choose r so that the resulting factor matrix pair has fewer parameters than the original matrix, ensuring a meaningful compression regime. In Table 1, we find that $p = 0.20$ (corresponding to $r = 19$) and $\lambda = 0.001$ performs best in terms of truncation–accuracy trade-offs.

ViT Hyperparameter Selection We selected each model’s learning rate based on the performance of the unmodified ViT model for each respective dataset. All ViT models were configured with an input resolution of 224×224 pixels and utilized patch size 16 for tokenization. LoRITA hyperparameter optimization was conducted through grid search with regularization parameter $\lambda \in \{10^{-1}, 10^{-2}, 10^{-3}, 10^{-4}\}$ and rank parameter $d \in \{1, 2, 3\}$ to ensure optimal performance. The best-performing configuration from three independent runs was selected for evaluation across additional datasets. LoRA was evaluated across various target ranks, with the proportion parameter p selected from $p \in \{0.05, 0.15, 0.3, 0.4, 0.5, 0.6, 0.7, 0.8, 0.9\}$. AdamQ3R underwent grid search optimization with regularization parameter $\lambda \in \{10^{-3}, 10^{-2}, 10^{-1}\}$ and proportion parameter $r \in \{0.05, 0.1, 0.15, 0.2\}$, with a stable *period* = 5. The regularization strength remained constant regardless of matrix dimensions. The QKV projection matrices were selected as the target for modification due to their prevalence in the literature as candidates for model compression and adaptation.

CIFAR-100 Data Augmentation For CIFAR-100 experiments, we applied comprehensive data augmentation during training, including random cropping with 4-pixel padding from the original 32×32 images, random horizontal flipping, and subsequent resizing to 224×224 pixels to match the ViT input requirements. Images were normalized using channel-wise means of (0.4914, 0.4822, 0.4465) and standard deviations of (0.2023, 0.1994, 0.2010), corresponding to the CIFAR-100 dataset statistics. The test set underwent only resizing to 224×224 pixels and the same normalization procedure, without augmentation.

Fine-Tuning Experimental Details We fine-tuned the pretrained RoBERTa-Base model (from Hugging Face) on all nine GLUE tasks using a maximum sequence length of 512 and a batch size of 16 (30 for CoLA). We run all fine-tuning experiments with a target rank as low as 4. The best performing setup had ‘reweighting period’ of 3 and $\lambda \in \{1.5, 2\}$. As shown in Table 3, we compare Q3R with LoRA and dense fine-tuning. The tasks and their metrics are summarized below:

- **Single-Sentence Classification**
 - CoLA: 8.5 k train / 1 k test; linguistic acceptability; Matthews correlation
 - SST-2: 67 k train / 1.8 k test; sentiment classification; accuracy
- **Similarity & Paraphrase**
 - MRPC: 3.7 k train / 1.7 k test; paraphrase detection; accuracy / F1
 - STS-B: 7 k train / 1.4 k test; sentence similarity; Pearson / Spearman correlation
 - QQP: 364 k train / 391 k test; question paraphrase detection; accuracy / F1
- **Natural Language Inference**
 - MNLI: 393 k train / 20 k matched + 20 k mismatched test; entailment classification; accuracy

- QNLI: 105 k train / 5.4 k test; question–answer entailment; accuracy
- RTE: 2.5 k train / 3 k test; textual entailment; accuracy
- WNLI: 634 train / 146 test; coreference-based inference; accuracy

D.2 Fine-tuning Experiments

To assess the potential of Q3R for fine-tuning large language models (LLMs), we conducted an additional experiment on Llama 3.2–3B using an NVIDIA A5000 GPU. Since the original meta-llama/Llama-3.2–3B checkpoint provides only the pretrained language model parameters, we instantiated the `LlamaForSequenceClassification` module, which attaches an additional linear projection, commonly referred to as the *classification head*, on top of the final hidden-state representation. This head, whose weight matrix is registered as `score.weight` (and optionally `score.bias`), is absent from the checkpoint and was therefore initialized with random Gaussian values.

The fine-tuning setup involves training this weight matrix as well as additive weights for the Q, K, and V layers.

With Q3R ($\lambda = 0.0001$, target rank = 4, for 100 epochs), we achieved an F1 score of 81.89% on the MRPC dataset of the GLUE benchmark, whereas full fine-tuning (effectively corresponding to setting $\lambda = 0$) resulted in an F1 score of 80.7% after the same number of epochs.

To further compare our proposed method, we conducted experiments on Llama3.2-1B on a subset of the GLUE tasks. Table 4 provides a comparison of our method’s performance with dense fine-tuning and LoRA.

Table 4: GLUE Benchmark Results for Llama3.2-1B

Model	MRPC	SST-2	RTE	CoLA	STS-B
Dense	86.3	95.3	77.3	47.09	90.5
LoRa rank=4	87.3	95.7	80.9	61.8	89.1
Q3R rank=4	87.8	94.4	64.7	51.8	87.04

We achieved the performance as mentioned in Table 4, with a single value of λ without any extensive hyperparameter search. While we acknowledge that better performance for GLUE tasks like RTE can often be obtained by starting from a more finely tuned initialization, these results demonstrate that the proposed method is effective even for the fine-tuning of large-scale LLMs.

D.3 Additional pre-training experiments

Table 5 and Table 6 demonstrate the low-rank induction techniques on ViT models. We train ViT-B on CIFAR-100 in Table 6 and ViT-T on CIFAR-10 in Table 5 respectively. A visual representation of the results in Table 5 is also illustrated in Figure 3 and that of Table 6 in Figure 2.

D.4 Computational Aspects

For some experiments (e.g., Q3R), we used an NVIDIA A5000 GPU to train the ViT models. The remainder of the experiments were performed on an NVIDIA V100 GPU with 32GB memory. The fine-tuning experiments were all performed on NVIDIA A5000 GPUs.

D.5 Computational Overhead of Methodology

In Algorithms 3 and 4, we provide the detailed stepwise FLOP count of our method. Following the experiments testing the influence of the reweighting period on the truncation, we report the average training time of the first 5 epochs below in Table 7. Note that regularization was only applied on the QKV matrices of a ViT-Tiny Transformer.

Based on the theoretical computational overhead outlined in Algorithms 1 and 3, along with the results above, we expect Q3R to incur additional computational and memory overhead in our (currently

Table 5: Performance at varying percentages of parameters saved on ViT-T when regularizer is applied to only attention blocks.

Model	15%	20%	30%	40%	50%	60%	70%	80%	90%	100%
Vanilla ViT-T	0.4687	0.5430	0.5892	0.6170	0.6542	0.6694	0.6726	0.6788	0.6892	0.7027
Q3R rank=4, $\lambda=0.01$	0.6032	0.6630	0.7043	0.7060	0.7084	0.7080	0.7079	0.7079	0.7077	0.7152
Q3R rank=9, $\lambda=0.01$	0.4852	0.5616	0.6668	0.6772	0.6831	0.6835	0.6832	0.6829	0.6831	0.7034
Q3R rank=14, $\lambda=0.01$	0.4576	0.5812	0.6866	0.6970	0.6988	0.7002	0.6997	0.6996	0.7003	0.7104
Q3R rank=19, $\lambda=0.01$	0.6208	0.6792	0.6913	0.6977	0.6978	0.6970	0.6970	0.6967	0.6966	0.7061
Q3R rank=4, $\lambda=0.001$	0.5694	0.6629	0.7017	0.7053	0.7084	0.7091	0.7086	0.7086	0.7079	0.7158
Q3R rank=9, $\lambda=0.001$	0.4214	0.5304	0.6467	0.6680	0.6691	0.6692	0.6691	0.6696	0.6695	0.6955
Q3R rank=14, $\lambda=0.001$	0.6040	0.6364	0.6642	0.6695	0.6695	0.6694	0.6698	0.6701	0.6704	0.6819
LoRITa D=1, $\alpha=0.1$	0.1154	0.1217	0.1234	0.1091	0.1502	0.2310	0.3377	0.4197	0.5027	0.7061
LoRITa D=1, $\alpha=0.001$	0.1576	0.1512	0.1602	0.1586	0.1902	0.2456	0.2955	0.3221	0.4056	0.7086
LoRITa D=1, $\alpha=0.01$	0.1474	0.1514	0.1539	0.1644	0.2486	0.2968	0.4150	0.4857	0.5326	0.6911
LoRITa D=2, $\alpha=0.01$	0.2478	0.2559	0.3115	0.4065	0.5127	0.5641	0.5997	0.6456	0.6720	0.7287
LoRITa D=2, $\alpha=0.1$	0.2041	0.2589	0.3639	0.5397	0.5982	0.6408	0.6727	0.6910	0.7025	0.7595
LoRITa D=2, $\alpha=0.001$	0.2195	0.2774	0.4163	0.5115	0.5461	0.5675	0.6137	0.6417	0.6614	0.7393
LoRITa D=3, $\alpha=0.01$	0.3794	0.5074	0.5907	0.6385	0.6598	0.6761	0.6843	0.6916	0.6959	0.7462
LoRITa D=3, $\alpha=0.001$	0.3951	0.5147	0.5952	0.6308	0.6639	0.6676	0.6798	0.6847	0.6833	0.7367
LoRA rank=4	0.3443	0.3443	0.3443	0.3443	0.3443	0.3443	0.3443	0.3443	0.3443	0.3443
LoRA rank=14	0.5859	0.5859	0.5859	0.5859	0.5859	0.5859	0.5859	0.5859	0.5859	0.5859

Table 6: CIFAR-100 Performance with ViT-B Attention Block Truncation

Model	5%	10%	15%	20%	30%	40%	100%
Vanilla ViT-B Best	0.2773	0.3355	0.3659	0.3909	0.4172	0.4327	0.4686
Q3R Best	0.3465	0.3979	0.4172	0.4301	0.4411	0.4485	0.4625
Q3R, rank=19, $\lambda=0.01$	0.3238	0.3979	0.4172	0.4301	0.4411	0.4485	0.4625
Q3R, rank=19, $\lambda=0.001$	0.3174	0.3790	0.3945	0.4050	0.4130	0.4197	0.4408
Q3R, rank=14, $\lambda=0.001$	0.3250	0.3978	0.4149	0.4240	0.4351	0.4429	0.4613
Q3R, rank=14, $\lambda=0.01$	0.3465	0.3950	0.4062	0.4172	0.4305	0.4389	0.4526
LoRITa Best	0.0607	0.1375	0.2003	0.2401	0.2975	0.3269	0.4111
LoRITa D=2, $\alpha=0.1$	0.0152	0.0444	0.0883	0.1404	0.2428	0.3043	0.4021
LoRITa D=3, $\alpha=0.001$	0.0607	0.1375	0.2001	0.2380	0.2975	0.3269	0.4103
LoRITa D=3, $\alpha=0.1$	0.0570	0.1369	0.2003	0.2401	0.2946	0.3188	0.4111

suboptimal) implementation. We attribute the lower reserved GPU memory to implementation differences in the optimizer.

E Ablation Studies

Table 8 presents the comparison between the regularization term (6) and Algorithm 2 evaluated across varied truncation levels and hyperparameters. Initially AdamQ3R presents competitive performance against Q3R; however, Q3R provides superior truncation performance on the validation set at lower truncation values (20% and below). The impact of the regularization parameter is notably small, with $\lambda = 0.001$ generally providing superior performance. We have used Algorithm 2 in our experiments as it provides more robustness to the hyperparameters as discussed in Section E.1.

E.1 Robustness to Hyperparameter Variations

Empirically, we found Q3R to be quite robust to its hyperparameters within reasonable ranges. Below, in Tables 9 and 10, we are providing few empirical evidences from Table 1 on ViT-Tiny. However, similar results can be conducted across other datasets and backbones as in Table 4 (CIFAR-100 on ViT-Base). Generally, when choosing λ , a viable rule is easy to tell if the choice of lambda is too small by monitoring if the Q3R value increases within the first few epochs. We recommend a value of λ that is slightly larger than the lower bound of the divergence threshold, as determining if the λ value is too large remains a challenge.

Table 7: Average training time (5 epochs) and reserved GPU memory for ViT-Tiny with QKV-only regularization.

Model	Variant / Setting	Avg. Time (s)	Reserved GPU Mem (GB)
Base	—	150.91	6.26
AdamQ3R	$T=500$	205.34	6.28
	$T=100$	207.39	6.31
	$T=50$	209.29	6.62
	$T=20$	217.90	8.22
	$T=10$	218.88	8.62
LoRA	$R=4$	124.83	11.89
	$R=14$	144.51	11.87
	$R=28$	145.28	11.89
Depth1 baseline	—	157.29	8.35

Table 8: Performance of Vit-T with AdamQ3R and Q3R across different truncation level on CIFAR10.

Model Name	5%	10%	15%	20%	30%	40%	100%
AdamQ3R, rank = 0.05*	0.1904	0.4600	0.6032	0.6630	0.7043	0.7060	0.7152
AdamQ3R, rank = 0.10*	0.2081	0.3591	0.4852	0.5616	0.6668	0.6772	0.7034
AdamQ3R, rank = 0.15*	0.1266	0.3970	0.4576	0.5812	0.6866	0.6970	0.7104
AdamQ3R, rank = 0.20*	0.1740	0.4717	0.6208	0.6792	0.6913	0.6977	0.7061
AdamQ3R, rank = 0.05^	0.2701	0.4608	0.5694	0.6629	0.7017	0.7053	0.7158
AdamQ3R, rank = 0.10^	0.1066	0.1741	0.4214	0.5304	0.6467	0.6680	0.6955
AdamQ3R, rank = 0.15^	0.2467	0.4993	0.6040	0.6364	0.6642	0.6695	0.6819
Adam w/ Q3R in loss, rank = 0.04*	0.2476	0.5171	0.6544	0.6862	0.6884	0.6874	0.6920
Adam w/ Q3R in loss, rank = 0.09*	0.1959	0.5040	0.6789	0.6789	0.6862	0.6870	0.6827
Adam w/ Q3R in loss, rank = 0.19*	0.2774	0.4317	0.6337	0.6697	0.6818	0.6896	0.6901
Adam w/ Q3R in loss, rank = 0.04^	0.2828	0.4699	0.6004	0.6569	0.6801	0.6801	0.6934
Adam w/ Q3R in loss, rank = 0.09^	0.3202	0.5527	0.6827	0.7024	0.7024	0.7079	0.7081
Adam w/ Q3R in loss, rank = 0.19^	0.3119	0.4440	0.6137	0.6670	0.6839	0.6877	0.6885

Legend: * Regularization parameter $\lambda = 0.01$, ^ Regularization parameter $\lambda = 0.001$

From Table 9, we observe that beyond the 20% retention point, the absolute accuracy gap never exceeds 0.3 percentage points between $\lambda = 0.001$ and $\lambda = 0.01$. This confirms that AdamQ3R is largely insensitive to λ within the 0.001–0.01 range in this practical operating regime.

E.1.1 Choice of Target Rank

Furthermore, in Table 10, we study the effect of the other hyperparameter, the target rank r_{target} . Here we scale the target rank by the layer dimensions so that a single hyper-parameter ρ works for networks of any size. For a weight matrix of shape $(m \times n)$ we set target rank $(r_{\text{target}}) = \rho \frac{m+n}{2mn}$. This definition makes the choice of r directly transferable across layers with different values of m and n .

From Table 10, we observe that once $\geq 30\%$ of the parameters are retained, the choice of rank changes accuracy by $\leq 3.8\%$, confirming low sensitivity to rank in this regime.

E.2 Choice of Reweighting Period

We observe in Table 11 that higher reweighting periods of $T = 300, 200$, and 100 result in underperformance in comparison to the lower reweighting periods, $T = 25, 5$. Although, longer reweighting periods provide some computational performance gains based upon formulation Algorithm 1, we observe superior performance for faster intervals which implies that frequent updates of the reweighting operator are more effective as it enforces the IRLS-majorisation of the logdet. In this regard, we recommend a reweighting period of $T = 5$ for the best performance from all the experiments that we have conducted.

Table 9: Effect of regularization strength λ on accuracy (%).

Parameter Retention	$\lambda = 0.001$	$\lambda = 0.01$
10%	46.08	46.30
15%	63.40	63.65
20%	66.30	66.40
30%	70.68	70.74
40%	71.04	71.09
100% (no trunc.)	71.95	71.52

Table 10: Effect of target rank r_{target} on accuracy for different parameter retention values.

Parameter retention	$\rho = 0.10$	$\rho = 0.15$	$\rho = 0.20$
5%	0.2322	0.1796	0.5606
10%	0.4085	0.4758	0.5883
15%	0.5606	0.4737	0.6175
20%	0.6295	0.4387	0.6511
30%	0.6526	0.3896	0.6749
40%	0.6654	0.4335	0.6833
100% (no trunc.)	0.6843	0.6737	0.6990

E.3 Merits of Low-Rank Initialization

In our experiments, we implemented spectral initialization where the regularized weight matrix has a rank greater than or equal to the target rank hyperparameter specified in Q3R. Our leading hypothesis for the poor validation accuracy following initialization is that Q3R imposes a strong constraint on the optimization landscape when the rank is low, thereby limiting the model’s capacity to explore more expressive solutions during training. This hypothesis is further supported by the fine-tuning results on RoBERTa in Table 3, where Q3R is applied to the pretrained model and continuously tuned on the GLUE benchmark tasks. We achieve notable results that support the general intuition that models tend to learn better representations through expressive architectures and training regimes. We experimented only on the smaller dataset to study how the initialization affects the performance of Q3R. We provide one example of empirical evidence on CIFAR-10 with ViT-Tiny, with $r = 0.05$ and $\lambda = 0.001$, in Table 12. We observe that low-rank initialization is unable to surpass the performance of Q3R without such a constraint on the initialization, as reported in Table 12. However, the accuracy lies within a 1% range of the full-rank initialized model, which shows that our proposed method can be implemented in a resource-constrained setup as well.

Code : The code is available at <https://github.com/ThatE10/q3r.git>.

Table 11: Model performance under different truncation percentages. Each model trained with $\lambda = 0.001$, $r = 0.2$, Trained for 30 epochs on CIFAR-10 with ViT-Tiny.

Model Name	5%	10%	15%	20%	30%	40%	100%
AdamQ3R, $T = 300$	0.2999	0.5609	0.6651	0.6801	0.6847	0.6838	0.6827
AdamQ3R, $T = 200$	0.2601	0.5914	0.6519	0.6766	0.6869	0.6885	0.6871
AdamQ3R, $T = 100$	0.2764	0.4871	0.6623	0.6776	0.6869	0.6885	0.6936
AdamQ3R, $T = 25$	0.3729	0.5813	0.6555	0.6725	0.6734	0.6778	0.6790
AdamQ3R, $T = 5$	0.1740	0.6838	0.6828	0.6949	0.6995	0.7000	0.7031

Table 12: Comparison of AdamQ3R with and without low-rank initialization.

Parameter retention	AdamQ3R + low-rank init.	AdamQ3R (Q3R, no low-rank init.)
15%	65.62	64.30
20%	68.30	69.60
30%	68.90	70.60
40%	69.26	70.84
100% (no trunc.)	70.02	72.19